Piston core record of Late Paleogene (31 Ma) to recent seafloor hydrothermal activity in the Southwest Pacific Basin

Andrea M. Stancin,[1] James D. Gleason,[1] Robert M. Owen,[1] David K. Rea,[1] and Joel D. Blum[1]

Received 11 December 2006; revised 22 October 2007; accepted 27 November 2007; published 1 March 2008.

[1] A large diameter piston core containing 8.35 m of metalliferous sediment has been recovered from a small abyssal valley in the remote Southwest Pacific Basin (31° 42.194′S, 143° 30° 331′W; 5082 m water depth), providing unique insight into hydrothermal activity and eolian sedimentation there since the early Oligocene. A combination of fish-teeth Sr-isotope stratigraphy and INAA geochemical data reveals an exponentially decreasing hydrothermal flux 31 Ma to the present. Although hydrothermal sedimentation related to seafloor spreading explains this trend, a complex history of late Eocene/early Oligocene ridge jumps, propagating rifts and plate tectonic reorganization of South Pacific seafloor could have also played a role. A possible hiatus in deposition, as recorded by changes in core composition just below 2 m depth, is beyond the resolution of the fish teeth Sr isotope dating method employed here; however, the timing of this interval may be coincident with extinction of the Pacific-Farallon Ridge at ~20 Ma. A low flux eolian component accumulating at this site shows an increase relative to the hydrothermal component above 2 m depth, consistent with dust-generating continental sources far to the west (Australia/New Zealand). This is the first long-term paleoceanographic record obtained from within the South Pacific "bare zone" (Rea et al., 2006), an anomalous region where Pacific seafloor has largely escaped sediment accumulation since the Late Cretaceous.

Citation: Stancin, A. M., J. D. Gleason, R. M. Owen, D. K. Rea, and J. D. Blum (2008), Piston core record of Late Paleogene (31 Ma) to recent seafloor hydrothermal activity in the Southwest Pacific Basin, *Paleoceanography*, *23*, PA1212, doi:10.1029/2006PA001406.

1. Introduction

[2] In February and March of 2005, scientists aboard the *R/V Melville* mapped a ~2 million square kilometer area of the SW Pacific Basin (Figure 1) that is almost entirely devoid of sediment [*Rea et al.*, 2006]. This region, known as the South Pacific Bare Zone (SPBZ), is unique among modern ocean basins both in terms of areal extent (approximately the size of the Mediterranean Sea) and duration of non-deposition (up to 80 million years). Several factors have collectively operated over the entire Cenozoic to produce this remarkable feature: extremely low biologic productivity in surface waters, a shallow CCD (carbonate compensation depth), and minimal eolian and hydrothermal inputs [*Rea et al.*, 2006]. These and other observations require that the sites surveyed over this vast area remained extremely remote from continental influence since the Late Cretaceous.

[3] Within the SPBZ, an anomalous 1 km^2 patch of sediment, ~24 m thick, was found atop 55 Ma oceanic crust [Site SP-9A; SPLAT Site Survey Report, unpublished; *Rea et al.*, 2006]. Situated within rough abyssal topography, this was the only significant sediment detected anywhere by seismic reflection at the survey site, which otherwise exhibited a complete absence of pelagic sediment drape [a chief characteristic of the SPBZ; *Rea et al.*, 2006]. A large 10 cm-diameter piston core recovered at this site (31° 42.194′S, 143° 30° 331′W; 5082 m water depth) captures thus far the only a long-term record of sediment accumulating anywhere within the SPBZ. Piston core MV0502-15JC (Site SP-9A, TUIM-03; Figure 1) contains 8.35 m of faintly mottled, very dark brown zeolitic clay (upper 2 m) and rust-red metalliferous clay (lower 6.35 m). The entire core is barren of microfossils, except for ubiquitous fish teeth, and no tephra layers were observed; thus, dating was not possible by conventional means.

[4] For this paper, we determined the Sr ichthyolith stratigraphy [*Gleason et al.*, 2002, 2004] of the core, and characterized the bulk geochemistry and radiogenic isotopic composition (detrital extract) of the sedimentary components. Building on the work of *Ingram* [1995], this study represents perhaps the first successful attempt to date an entirely metalliferous sediment core by fish teeth stratigraphy, here revealing a near-continuous depositional record extending back to the Early Oligocene. The origin of the hydrothermal and detrital sedimentary components at this site, which is itself an anomalous domain within the SPBZ, are then discussed within the context of known, though sparse, paleoceanographic records from elsewhere within the SW Pacific Basin. We conclude that the Cenozoic evolution of this portion of the Southwest Pacific Basin can be better elucidated by further studies of metalliferous cores, both from within and around the periphery of the SPBZ.

2. Methods

[5] Because of the dearth of microfossils and the very low pelagic sedimentation rates recorded at this site and else-

[1]Department of Geological Sciences, University of Michigan, Ann Arbor, Michigan, USA.

0883-8305/08/2006PA001406

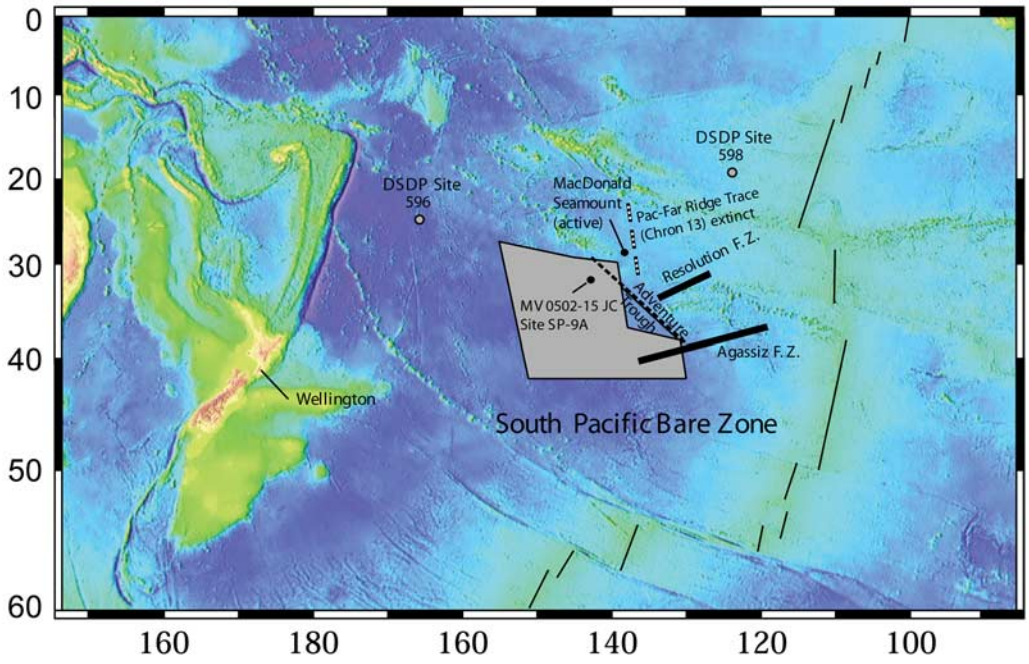

Figure 1. Map of the SW Pacific Basin, showing position of Site SP-9A and piston core MV0502-15JC (31° 42.194′S, 143° 30° 331′W, 5082 m water depth) on 55 Ma crust (Chron 25), with various tectonic features and drill sites highlighted within and near the South Pacific Bare Zone [grey area; *Rea et al.*, 2006]. Location of Pacific-Farallon ridge at 33 Ma (magnetic chron 13 from *Tebbens and Cande* [1997]). Trace of East Pacific and Pacific-Antarctic Rise also shown. Base map courtesy of the USGS from NOAA's ETOPO2 Global 2′ Elevations data set.

where within the SPBZ, the core required dating using fish teeth Sr isotope stratigraphy [*Ingram*, 1995; *Gleason et al.*, 2002, 2004]. Twelve intervals were selected for dating. Fish teeth were hand picked and individually cleaned using the method adopted by *Gleason et al.*, [2002]. The procedure consisted of (1) a reductive cleaning step to remove Fe-Mn oxide coatings (Figure 2) by a combination of sodium citrate, sodium dithionite and sodium bicarbonate, followed by (2) an oxidative cleaning step to remove organics and biogenic silica using dilute sodium hydroxide and hydrogen peroxide, and (3) a carbonate removal step, where the teeth are briefly subjected to a dilute acetic acid bath [*Gleason et al.*, 2002]. Any remaining contaminants were removed by multiple rinses with.001N nitric acid in micro-centrifuge tubes.

[6] After complete cleaning, fish teeth appeared white or translucent, with no visible opaque material (Figure 2). Teeth were then dissolved in 3N nitric acid and centrifuged before Sr was isolated by column chemistry [*Gleason et al.*, 2002, 2004]. The Sr was loaded on tungsten filaments with tantalum oxide activator and analyzed in static mode on a TIMS multicollector Finnigan MAT 262 Mass Spectrometer

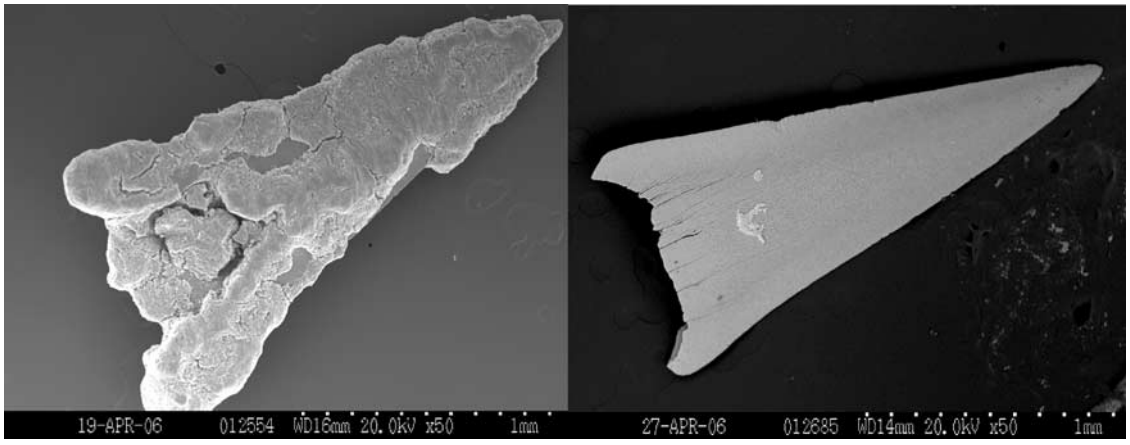

Figure 2. SEM image of a 1.5 mm long fish tooth, interval 102–104 cmbsf, MV0502-15JC, before (left) and after (right) removal of hydrogenous Mn-rich coatings.

at the University of Michigan. Signal intensity on Sr was typically 1.5–2.0 V on mass 88, but varied depending on the size and quantity of teeth processed. Isotopic ratios were normalized online to $^{86}Sr/^{88}Sr = 0.1194$ using an exponential law fractionation algorithm, and are reported as the mean with standard deviation on 100 to 200 ratios collected during a typical run. The NBS (NIST) 987 Sr isotopic standard gave $^{87}Sr/^{86}Sr = 0.710246 \pm 12$ (n = 29), requiring no corrections. Ages were assigned to each interval by comparing the fish tooth Sr isotope ratios in MV0502-15JC to the LOWESS statistical fit (calibrated to the NBS 987 value of $^{87}Sr/^{86}Sr = 0.710248$) for Cenozoic seawater Sr isotopic composition [*McArthur et al.*, 2001].

[7] Bulk sediment chemistry was determined by Instrumental Neutron Activation Analysis (INAA). Twenty-six bulk samples were selected from the core and rinsed in triple distilled water three times to remove any excess seawater Na prior to irradiation, freeze dried, and one gram weighed out. In the process, it was noted that samples from 243 cm and deeper were a very different consistency than the core top. Upon contact with water, the sediment disaggregated, releasing a stream of bubbles into the vial. This sediment bore a striking resemblance to metallic rust. Weighed samples of approximately 1 g each, along with two rock standards, were sent to Oregon State University for INAA to determine trace metal and REE abundances. The data for elements with intermediate and long half-life isotopes (including As, Ba, La, Lu, K, Na, Sm, U, Yb, Ce, Co, Cr, Cs, Eu, Fe, Hf, Nd, Rb, Sc, Sr, Ta, Tb, Th, Zn, Zr), result from a 7-h irradiation in the rotating rack facility, which experiences an average thermal neutron flux of 2×10^{12} n/cm^2/s. Following irradiation, two separate counts of gamma activity are done: a 5000-second count (live time) of each sample after a 1-week decay period, and a 10,000-second count (live time) after a period of 4 weeks decay.

[8] In contrast, the data for short half-live isotopes (Al, Ca, Ti, V, K, Mn, Na) result from a 1-min irradiation delivered via pneumatic tube to an in-core location; because of the high Mn concentrations these were run at relatively low power, with an average thermal flux of 10^{11} n/cm^2/s. Again, two separate counts were taken, one after a13-min decay (for Al, Ca, Ti, and V) and a second count after 2-h decay (for Dy, Mn, K, and Na); both counts were for 575 s. Not all elements typically reported by INAA (e.g., Ti) could be measured because of the large interference from Mn.

[9] Elemental concentrations were determined through direct comparison on a weight-ratio basis with appropriate standard reference materials. For most elements, concentrations were based on comparison with three replicates of the standard reference material NIST1633A (coal fly ash). Determination of Ca content was based on NIST688 (basalt rock), and NIST1649 (urban particulate) was utilized for the determination of Br, Na, and Zn. Contents of precious metals were evaluated relative to a mixed liquid AA standard (100 ppm) pre-dried on filter paper. Analytical uncertainties are indicated in Table 1. Unless noted otherwise, all data reductions are based on NIST certified values for the standard reference materials. Two blind rock standards were included: PACMUD, an in-house (Michigan) reference material [*Owen and Ruhlin*, 1986] and the USGS standard MAG-1 [*Govindaraju*, 1994]. The correlation for both standards between accepted and measured values was considered quite good (Table 1).

[10] The detrital (terrigenous) sediment component was extracted for radiogenic isotopic analysis following the procedures of *Rea and Janecek* [1981] and *Hovan* [1995]. The sediment was first sieved at 63 μm and then subjected to acetic acid treatment to remove any carbonate. Authigenic oxides were removed with sodium bicarbonate, sodium citrate and sodium dithionite. Opal and organics were removed with a sodium hydroxide solution. The remaining material was rinsed with distilled water and wet-sieved at 38 μm and then cleaned further with ammonium acetate (1M) before freeze drying. The Sr and Nd isotopic compositions of the detrital extract were determined at Michigan by TIMS using methods described by *Stancin et al.* [2006]. REE (rare Earth element) patterns on a subset of the <38 micron detrital extract (3 intervals) were determined by ICP-MS at Michigan using methods of *Gleason et al.* [2004] to check for any remaining hydrogenous component.

3. Results

3.1. Age Model and Sedimentation Rates

[11] Fish teeth Sr isotopic compositions (Figure 3a) and computed ages for core MV0502-15JC (Figure 3b) are shown in Table 2. The base of the core at 8.23 m below seafloor (mbsf) was determined to be 31.32 ± 0.8 Ma, which is early Oligocene in age (Figure 3b). Age uncertainties assigned by this method for this part of the Cenozoic timescale tend to be fairly low, because of the steep slope in the marine Sr isotope curve [*McArthur et al.*, 2001]. Using this age for the core base, and assuming a linear sedimentation (LSR) rate with no hiatuses, an *average* LSR of 0.27 mm/ka was computed for the total core, comparable to pelagic clay sedimentation rates in other parts of the Pacific [e.g., *Rea et al.*, 1985; *Zhou and Kyte*, 1992; *Kyte et al.*, 1993; *Gleason et al.*, 2002]. However, the Sr isotope stratigraphy reveals an order of magnitude decrease in sedimentation rates between 4.43 mbsf and 1.43 mbsf (Table 2 and Figure 3b). From this information, the LSR calculated for the interval between 8.23 mbsf (31.3 Ma) and 5.53 mbsf (~30 Ma) is 2.00 mm/ka, while the interval between 0.83 mbsf (~17 Ma) and the core top (0 Ma) has an average LSR of 0.05 mm/ka. The combined fish teeth age data closely describe an exponential equation of y = 5.9013 * e^(0.15641×), which we interpret to most accurately represent the age-depth function of this core (Figure 3b). An exponential decay in bulk sedimentation rate is expected in these types of settings, and has been described previously for deep-sea locations where hydrothermal precipitates constitute the dominant sedimentary component [*Dickens and Owen*, 1995]. The fact that the core top did not yield (within error) a precise modern Sr isotopic composition ($^{87}Sr/^{86}Sr = 0.70916$) could be due to core disturbance at the top coupled with the low sedimentation rate [*Doyle and Riedel*, 1979].

3.2. Results of Bulk Sediment Chemical Analysis

[12] The results of the bulk INAA analysis are shown in Table 1. Elements strongly enriched in "distal" type sea-

Table 1. Bulk INAA Data for Piston Core MV0502-15JC

Sample MV0502-15JC	Al *ppm*	±1σ	As *ppm*	±1σ	Ba *ppm*	±1σ	Br *ppm*	±1σ	Ce *ppm*	±1σ	Co *ppm*	±1σ	Cr *ppm*	±1σ	Cs *ppm*	±1σ	Eu *ppm*	±1σ	Fe *ppm*	±1σ	Hf *ppm*	±1σ
cmbsf																						
0-2	80,387	4,115	67.23	4.20	1,793.32	107.75	14.85	0.65	250.40	4.90	302.73	9.51	36.07	2.54	6.08	0.36	9.06	0.24	84,311	581	6.49	0.31
22–24	82,611	4,401	63.78	4.00	1,441.06	88.41	35.51	0.75	235.56	4.62	298.01	9.36	41.35	2.58	5.42	0.31	7.41	0.20	81,177	561	6.44	0.32
42–44	76,700	3,991	65.87	4.13	1,131.35	75.03	17.14	0.69	263.73	5.15	338.81	10.64	46.24	3.09	6.22	0.36	9.26	0.25	88,487	604	6.88	0.33
82–84	73,921	3,946	67.33	4.21	1,024.58	74.81	31.78	0.82	232.18	4.56	322.64	10.14	38.43	2.62	5.91	0.33	6.10	0.17	83,581	568	6.40	0.30
102–104	76,370	4215	61.22	3.95	1,386.73	88.51	33.91	0.76	239.56	4.71	320.74	10.08	43.28	3.02	5.36	0.33	8.82	0.24	78,902	556	6.00	0.31
142–144	83,617	4435	63.85	4.09	971.09	71.23	26.25	0.89	252.56	4.94	344.76	10.83	44.86	2.87	5.43	0.33	8.70	0.24	80,359	561	6.52	0.33
182–184	78,729	4,866	74.39	4.75	764.04	65.68	50.37	0.99	262.89	5.14	366.89	11.52	40.16	3.03	5.63	0.35	9.20	0.25	88,218	609	6.54	0.32
202–204	75,087	4,032	76.79	4.86	527.23	55.34	26.87	0.85	271.30	5.28	383.26	12.04	41.67	2.77	5.18	0.33	9.26	0.25	87,233	604	6.96	0.33
242–244	66,590	4,028	150.87	9.25	480.31	67.79	7.77	0.90	330.19	6.41	452.16	14.20	20.82	3.02			16.15	0.43	127,684	801	6.93	0.35
262–264	66,243	4,261	147.25	9.05	422.16	57.60	24.33	0.98	334.13	6.48	463.06	14.54	20.59	2.78			16.38	0.43	130,110	810	6.80	0.36
302–304	62,696	3,839	187.00	11.45	406.76	61.63	9.36	0.88	378.09	7.29	487.26	15.30	20.85	3.17			19.75	0.52	147,268	908	7.20	0.37
342–344	59,489	5,232	222.09	13.55	463.65	68.34	16.77	1.07	380.83	7.36	501.52	15.74	15.22	2.80			20.21	0.53	162,504	969	8.28	0.37
362–364	50,830	4,943	226.78	13.85	474.11	69.72	20.00	1.27	419.02	8.05	405.59	12.74	15.28	3.05			25.82	0.67	162,941	977	7.86	0.40
422–424	45,441	3,396	278.97	16.94	370.03	61.14	8.16	1.01	399.93	7.69	368.50	11.57	18.53	3.40			20.90	0.55	201,100	1,161	8.48	0.39
442–444	40,264	4,160	363.45	21.95	518.22	68.46	7.06	0.99	397.78	7.64	324.89	10.21	15.09	2.95			19.83	0.52	245,290	1,382	9.48	0.41
482–484	44,476	3,397	376.59	22.65	405.52	60.47	7.55	0.87	303.06	5.93	235.26	7.40	12.97	2.61			17.44	0.46	299,024	1,647	9.14	0.41
522–524	42,369	3,459	407.67	24.50	480.55	59.19	15.91	0.99	302.69	5.93	234.44	7.38		0.12			17.22	0.46	316,545	1,736	8.73	0.42
552–554	33,535	2,892	445.00	26.67	475.89	61.21	9.03	0.72	274.72	5.41	200.18	6.30	17.87	2.74			17.79	0.47	319,388	1,744	7.98	0.36
572–574	34,055	3,295	443.02	26.55	479.36	63.65	9.73	0.81	275.03	5.42	213.72	6.73	12.24	2.55			15.89	0.42	316,622	1737	7.41	0.34
612–614	30,988	2,771	465.11	27.87	640.97	70.22	7.63	0.73	289.36	5.69	231.26	7.28	13.84	2.39			16.54	0.44	337,699	18,44	7.59	0.36
642–644	32,593	3,273	456.66	27.38	684.13	70.70	8.89	0.80	287.88	5.65	221.99	6.99	16.07	2.97			15.81	0.42	322,446	1,762	7.27	0.35
682–684	29,497	3,765	457.72	27.45	729.39	74.62	8.39	0.78	296.87	5.81	223.24	7.02		0.11			16.55	0.44	336,272	1,834	7.36	0.37
702–704	31,280	4,331	454.64	27.27	720.75	72.03	6.52	0.85	274.70	5.41	218.83	6.89	20.80	2.97			16.43	0.44	322,988	1,768	6.44	0.35
742–744	33,142	4,376	426.79	25.60	815.13	69.67	12.71	0.90	267.20	5.27	202.38	6.37	12.17	2.49			14.91	0.40	305,977	1,680	6.42	0.34
782–784	30,216	3,242	430.02	25.81	772.23	75.60	8.79	0.83	400.12	7.70	288.32	9.07	17.20	3.03			22.33	0.59	273,419	1,525	9.21	0.40
822–824	23,619	3,409	390.75	23.47	797.76	72.24	7.05	0.75	340.93	6.61	264.47	8.32	15.72	3.11			18.09	0.48	286,786	1,589	9.38	0.42
USGS MAG-1	**86,056**	3,994	**10.33**	1.00	**468.66**	51.33	**226.13**	1.01	**90.06**	1.96	**21.45**	0.70	**101.72**	2.78	**8.76**	0.36	**1.43**	0.05	**48,021**	346	**4.18**	0.22
Accepted[a]	86,637		9.20		479.00		252.00		88.00		20.40		97.00		8.60		1.55		47539		3.70	
Interlab std.			56.34	3.43	353.20	32.01	41.62	0.45	10.06	0.72	19.86	0.65					1.08	0.04	59,795	395	0.46	0.09
Accepted			57.8[b]		368[c]		44.8[d]		10[b]		20[b]						1.19[b]		61200[c]		0.30[d]	

[a] *Govindaraju*, 1994.
[b] *Dickens and Owen*, 1995 (Table 2 - Measured).
[c] *Owen and Ruhlin*, 1986 (Tables 1/2 - Mean) also: *Dickens and Owen*, 1995 (Table 2 - Published).
[d] *Owen and Ruhlin*, 1986 (Tables 1/2 UM).
[e] *Owen and Ruhlin*, 1986 (Tables 1/2 OSU).
[f] calculated from chondrite-normalized values.
[g] calculated from formula used by *Dickens and Owen*, 1995.

Table 1. (continued)

La		Lu		Mo		Mn		Nd		Sb		Sc		Sm		Tb		Th		U	
ppm	±1σ	*ppm*	±1σ	*ppm*	±1σ	*ppm*	±1σ	*ppm*	±1σ	*ppm*	±1σ	*ppm*	±1σ	*ppm*	±1σ	*ppm*	±1σ	*ppm*	±1σ	*ppm*	±1σ
144.28	7.95	3.02	0.29	43.23	3.25	21,860	259	176.16	22.69	5.52	0.28	27.92	0.96	42.00	2.15	6.58	0.48	22.72	0.33	2.39	0.36
117.44	6.47	2.42	0.23	44.65	3.28	21,117	252	127.45	18.17	5.37	0.26	25.17	0.87	33.89	1.74	5.30	0.40	19.12	0.28	2.57	0.35
128.52	7.08	2.60	0.25	47.71	3.47	22,443	266	158.03	21.37	6.19	0.31	28.61	0.99	37.38	1.91	6.48	0.47	21.91	0.35	2.83	0.38
103.01	5.68	2.14	0.20	52.13	3.68	20,205	240	125.26	17.00	5.30	0.27	24.87	0.86	29.38	1.51	4.41	0.35	16.68	0.30	2.86	0.35
129.64	7.14	2.77	0.26	43.14	3.18	22,082	263	169.79	22.48	5.22	0.27	26.84	0.93	38.40	1.97	6.04	0.44	19.94	0.31	2.12	0.37
131.71	7.26	2.73	0.26	51.56	3.71	23,315	277	172.14	22.06	5.45	0.27	26.33	0.91	39.19	2.01	6.02	0.44	19.46	0.29	1.93	0.34
143.86	7.93	2.99	0.28	56.26	3.97	23,986	286	165.79	22.21	5.95	0.30	28.35	0.98	41.97	2.15	6.00	0.44	19.17	0.29	2.39	0.40
143.86	7.93	2.92	0.28	61.91	4.34	24,213	287	190.97	24.82	6.14	0.32	27.38	0.94	43.47	2.23	6.92	0.50	19.24	0.35	2.46	0.36
279.58	15.40	5.41	0.51	117.69	7.80	37,837	446	304.81	37.58	10.74	0.47	38.87	1.34	71.18	3.64	11.85	0.82	18.95	0.35	5.09	0.51
271.62	14.96	5.17	0.49	112.12	7.46	36,265	429	330.68	40.47	10.49	0.46	39.24	1.35	69.67	3.57	12.02	0.83	17.44	0.33	4.91	0.51
326.78	17.99	5.98	0.57	128.61	8.51	36,289	427	346.25	41.98	12.51	0.51	43.71	1.51	84.08	4.31	13.96	0.96	17.58	0.34	6.06	0.56
336.40	18.52	6.06	0.57	131.31	8.65	34,017	552	372.16	44.55	13.34	0.54	44.26	1.52	87.78	4.49	14.83	1.01	18.99	0.36	6.02	0.59
409.33	22.54	7.35	0.69	127.87	8.55	41,457	673	518.80	63.45	14.65	0.57	51.43	1.77	107.20	5.49	18.78	1.26	23.37	0.39	6.91	0.61
346.32	19.07	5.60	0.53	129.17	8.59	40,497	476	377.43	45.58	15.45	0.60	44.06	1.52	84.53	4.33	14.41	0.99	14.38	0.34	5.57	0.54
346.69	19.09	5.66	0.54	155.17	10.15	40,076	471	351.47	42.63	18.15	0.68	42.84	1.48	81.53	4.18	13.69	0.93	12.90	0.33	7.47	0.61
372.60	20.51	6.22	0.58	143.73	8.94	45,403	533	306.41	33.82	20.48	0.76	38.32	1.32	87.98	4.49	11.53	0.80	8.05	0.25	7.30	0.57
322.54	17.75	5.38	0.50	155.19	9.62	43,266	508	266.73	29.58	19.73	0.73	38.21	1.32	74.91	3.83	11.81	0.82	8.33	0.27	6.84	0.52
330.00	18.16	5.57	0.52	153.25	9.46	39,943	470	295.30	32.89	19.84	0.73	36.48	1.26	75.22	3.84	11.75	0.82	7.57	0.27	8.28	0.53
313.90	17.28	5.27	0.49	143.90	8.91	43,659	513	289.54	31.76	18.85	0.70	34.19	1.18	70.51	3.60	10.96	0.77	6.51	0.24	7.01	0.50
343.64	18.91	5.56	0.52	145.57	9.02	42,988	505	268.15	30.51	20.49	0.76	35.67	1.23	75.51	3.86	11.51	0.81	8.46	0.28	8.01	0.54
318.55	17.53	5.20	0.49	162.55	10.02	48,639	571	272.44	30.36	20.23	0.74	34.30	1.18	69.35	3.54	10.39	0.74	8.45	0.28	6.76	0.51
320.95	17.66	5.14	0.48	153.14	9.44	49,959	586	256.91	28.85	21.15	0.78	35.46	1.22	68.39	3.49	10.94	0.77	8.49	0.26	6.98	0.51
324.30	17.85	5.08	0.48	159.19	9.84	51,012	599	251.76	28.19	21.00	0.77	34.72	1.20	69.88	3.57	10.89	0.77	8.75	0.28	6.82	0.52
307.84	16.94	4.75	0.44	166.85	10.25	54,549	640	255.12	28.62	19.04	0.72	32.60	1.12	67.70	3.46	9.76	0.69	7.89	0.24	6.57	0.48
313.86	17.28	4.82	0.45	167.12	10.27	53,821	631	252.90	28.22	21.16	0.78	46.27	1.59	69.28	3.54	14.98	1.03	13.39	0.30	6.04	0.48
275.02	15.14	4.17	0.39	149.64	9.22	52,261	613	221.02	24.92	19.89	0.74	40.15	1.38	60.91	3.11	12.35	0.86	9.95	0.28	5.26	0.46
46.67	2.58	**0.47**	0.05	**1.50**	0.73	**780**	14	**43.36**	8.40	**1.15**	0.12	**16.91**	0.58	**8.24**	0.42	**1.07**	0.15	**11.70**	0.20	**3.13**	0.29
43.00		0.40		1.60		775		38.00		0.96		17.20		7.50		0.96		11.90		2.70	
27.71	1.53	0.47	0.05	30.44	1.98	12,424	149		0.95	2.37	0.14	1.53	0.06	4.47	0.23	0.75	0.10	0.27	0.07	1.53	0.25
29.2[b]		0.42[b]		31[b]		12300[e]				2.28[b]		1.7[b]		4.4[b]		0.84[b]				1.26[d]	

Table 1. (continued)

V		Yb		Zn		Al_2O_3		Na_2O		MnO		Fe_3O_4		Fe_2O_3	FeO		Ce/Ce*	Ce/Ce*
ppm	±1σ	*ppm*	±1σ	*ppm*	±1σ	*wt.%*	±1σ	*wt.%*	±1σ	*wt.%*	±1σ	*wt.%*	±1σ	*wt.%*	*wt.%*	Fe/Sc	Chon.[f]	ASC[g]
										cmbsf								
198.21	34.3	19.62	1.10	209.6	9.5	15.19	0.78	2.66	0.02	2.82	0.01	11.65	0.08	12.05	10.85	3020	0.767	0.675
270.89	38.5	16.57	0.94	188.0	9.2	15.61	0.83	2.81	0.02	2.73	0.01	11.22	0.08	11.61	10.44	3226	0.922	0.782
206.95	35.0	17.71	0.99	199.3	9.5	14.50	0.75	2.44	0.02	2.90	0.01	12.23	0.08	12.65	11.38	3093	0.905	0.798
189.56	31.0	13.56	0.78	173.7	9.3	13.97	0.75	2.71	0.02	2.61	0.01	11.55	0.08	11.95	10.75	3361	0.997	0.882
263.35	42.2	17.99	1.01	196.2	9.3	14.43	0.80	2.90	0.03	2.85	0.01	10.90	0.08	11.28	10.15	2939	0.798	0.715
275.07	39.7	17.88	1.00	204.3	9.5	15.80	0.84	2.53	0.02	3.01	0.01	11.11	0.08	11.49	10.34	3052	0.828	0.741
264.36	40.2	19.90	1.13	215.5	9.5	14.88	0.92	3.40	0.03	3.10	0.01	12.19	0.08	12.61	11.35	3112	0.823	0.710
322.30	48.0	19.50	1.09	216.0	10.1	14.19	0.76	2.68	0.03	3.13	0.01	12.06	0.08	12.47	11.22	3186	0.810	0.726
474.98	53.8	35.63	2.00	365.8	12.9	12.59	0.76	2.02	0.03	4.89	0.01	17.65	0.11	18.26	16.43	3285	0.542	0.477
371.87	47.5	34.21	1.92	339.0	12.3	12.52	0.81	2.51	0.03	4.68	0.01	17.98	0.11	18.60	16.74	3316	0.544	0.496
400.36	43.7	39.73	2.22	400.8	13.2	11.85	0.73	2.16	0.03	4.69	0.01	20.35	0.13	21.06	18.95	3370	0.536	0.466
445.06	44.5	41.00	2.30	416.9	14.1	11.24	0.99	2.01	0.03	4.39	0.02	22.46	0.13	23.23	20.91	3671	0.517	0.454
516.22	45.4	49.45	2.76	469.4	14.9	9.61	0.93	2.45	0.04	5.35	0.02	22.52	0.14	23.30	20.96	3168	0.447	0.410
704.74	53.7	38.23	2.14	470.4	13.5	8.59	0.64	1.13	0.03	5.23	0.01	27.79	0.16	28.75	25.87	4564	0.530	0.471
781.61	63.1	38.88	2.18	567.0	13.4	7.61	0.79	1.12	0.04	5.17	0.01	33.90	0.19	35.07	31.56	5726	0.539	0.510
837.19	59.9	40.49	2.27	769.7	15.1	8.41	0.64	1.04	0.03	5.86	0.01	41.33	0.23	39.09	35.18	5909	0.410	0.475
850.05	57.2	34.09	1.91	749.0	14.7	8.01	0.65	1.29	0.03	5.59	0.01	43.75	0.24	41.00	36.89	7143	0.472	0.377
894.39	54.8	35.73	2.00	797.1	14.9	6.34	0.55	0.90	0.02	5.16	0.01	44.14	0.24	42.75	38.47	7804	0.408	0.381
1074.31	67.4	33.38	1.87	712.3	14.2	6.44	0.62	0.82	0.02	5.64	0.01	43.76	0.24	45.26	40.72	8284	0.425	0.402
941.01	54.1	35.82	2.01	726.5	14.2	5.86	0.52	0.65	0.02	5.55	0.01	46.67	0.25	45.66	41.09	8754	0.432	0.335
1061.68	67.9	33.17	1.86	725.5	14.0	6.16	0.62	0.68	0.02	6.28	0.01	44.56	0.24	45.27	40.73	9259	0.450	0.362
1055.47	62.4	32.67	1.83	800.8	14.7	5.57	0.71	0.62	0.02	6.45	0.01	46.47	0.25	48.28	43.44	9468	0.471	0.380
1063.08	58.1	32.81	1.84	736.6	13.9	5.91	0.82	0.59	0.02	6.59	0.01	44.64	0.24	46.10	41.48	9402	0.435	0.373
1096.78	66.2	31.48	1.77	738.5	13.9	6.26	0.83	0.79	0.02	7.04	0.01	42.29	0.23	48.08	43.26	9484	0.436	0.404
1040.71	65.3	31.33	1.76	707.1	15.4	5.71	0.61	0.80	0.02	6.95	0.01	37.79	0.21	46.18	41.55	9302	0.647	0.366
1156.74	70.9	27.45	1.55	685.9	14.8	4.46	0.64	0.68	0.02	6.75	0.01	39.63	0.22	43.75	39.36	9387	0.630	0.406
159.58	18.3	**2.62**	0.18	**154.4**	5.4	**16.26**	0.75	**4.37**	0.02	**0.100**	0.01	**6.64**	0.05					
140.00		2.60		154.5		16.37		3.83		0.098		6.57						
226.99	25.2	2.93	0.18	141.8	4.6			1.13	0.01		0.01	8.26	0.05					
220[e]		3[b]		142[b]								8.46[c]						

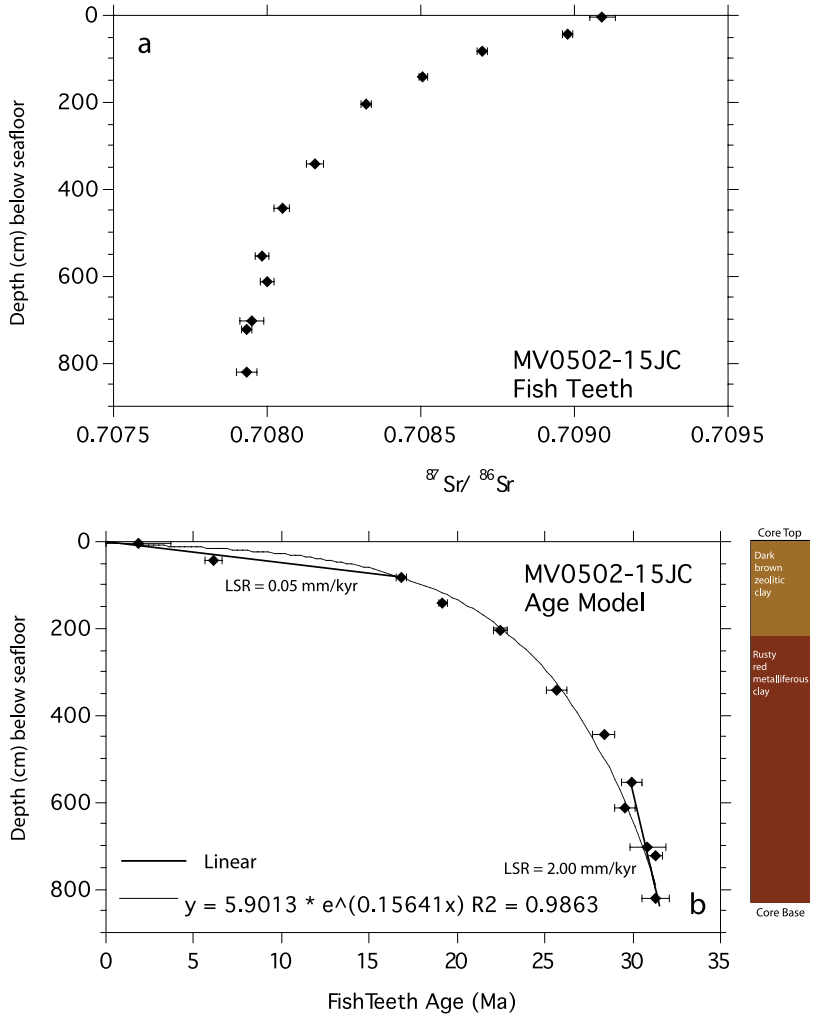

Figure 3. $^{87}Sr/^{86}Sr$ isotope ratios (a) and age model (b) for core MV0502-15JC ichthyoliths (determined from LOWESS seawater fit of *McArthur et al.*, 2001). Base of core is 31 Ma, with a rapid decrease in sedimentation rates recorded between ~28 and ~19 Ma. Average linear sedimentation rates (LSR) calculated from the Sr ichthyolith age model vary between 2.00 mm/ka (core base) and <0.05 mm/ka (core top). An exponential fit to the fish teeth age data yields an r^2 value of 0.9863 for a preferred age-depth model. Core log at right shows a pronounced lithologic change at about 2 m depth (see text).

Table 2. Fish Teeth Sr Isotope Ratios and Ages by TIMS for Piston Core MV0502-15JC

Depth, cmbsf	$^{87}Sr/^{86}Sr$ (measured)[a]	2SE (±)[b]	Age, Ma[c]	Age (low), Ma[3]	Age (high), Ma[3]
3	0.709090	0.000041	1.84	0.68	4.45
43	0.708978	0.000019	6.10	5.87	6.60
83	0.708698	0.000017	16.82	15.56	17.05
143	0.708508	0.000015	19.17	18.95	19.42
203	0.708328	0.000015	22.48	22.07	22.88
343	0.708156	0.000027	25.67	25.15	26.23
443	0.708049	0.000026	28.35	27.69	29.01
553	0.707985	0.000023	29.96	29.39	30.57
613	0.708000	0.000024	29.59	28.99	30.19
703	0.707951	0.000038	30.87	29.86	31.81
723	0.707936	0.000017	31.27	30.82	31.67
823	0.707934	0.000032	31.32	30.46	32.05

[a]Normalized to $^{86}Sr/^{88}Sr = 0.1194$.
[b]Instrumental (measured) error.
[c]*McArthur et al.*, 2001 (LOWESS) NBS987 $^{87}Sr/^{86}Sr = 0.710246 \pm 0.000012$ (n = 29; U. Michigan, early 2006).

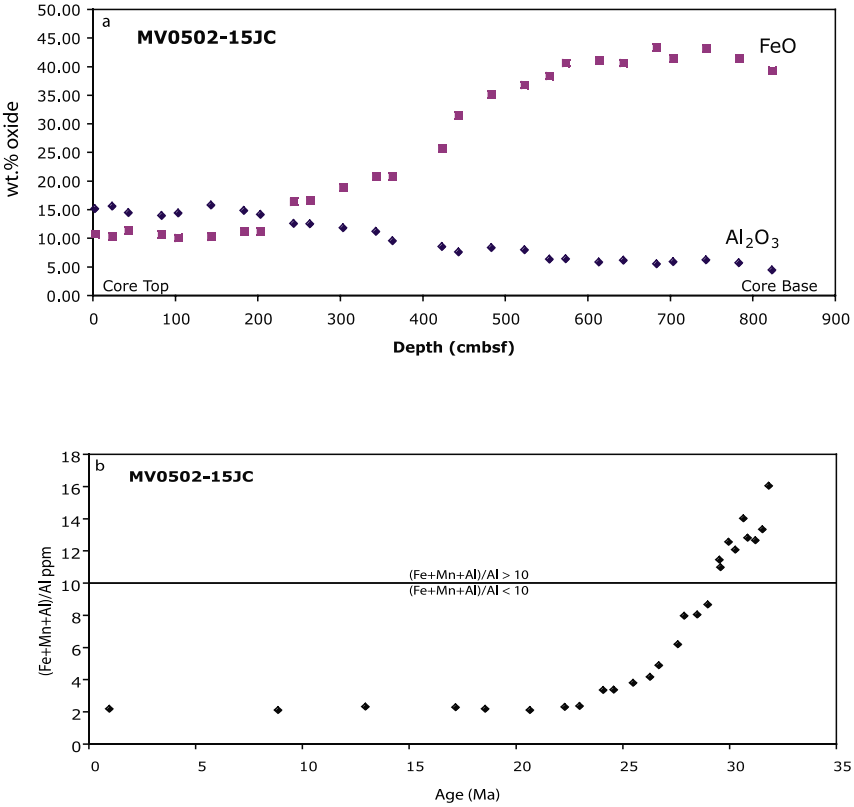

Figure 4. FeO and Al_2O_3 versus Depth (a) and (Fe + Mn + Al)/Al versus Age (b) in MV0502-15JC. The crossover point in abundances of Fe versus Al occurs at 2 mbsf (~20 Ma). (Fe + Mn + Al)/Al is greater than 10 in the lower part of the core, consistent with sedimentation associated with modern mid-ocean ridge environments [*Mills and Elderfield*, 1995]. Down core mass accumulation rates (MAR) of the hydrothermal component can be estimated from the abundances of Al (terrigenous) and Fe (hydrothermal) by the proportion $MAR_H \alpha C_H/C_T$ [*Dickens and Owen*, 1995], assuming constant terrigenous flux and dry bulk density (DBD) values. Combined with information from the age model, calculated MAR_H varies over nearly two orders of magnitude (see Supplementary Documents).

floor hydrothermal sediments [e.g., *Lyle et al.*, 1986, 1987; *Klinkhammer and Hudson*, 1986; *Marchig et al.*, 1987; *Marchig and Erzinger*, 1986; *Dickens and Owen*, 1995; *Mills and Elderfield*, 1995; *German et al.*, 1999] include Fe, As, Sb, V, Zn, and Mn, all of which co-vary in this data set. Fe/V (r = 0.97), Fe/Zn (r = 0.98) and Fe/As (r = 0.98) ratios are particularly invariant in MV0502-15JC, with As, Sb, V, and Zn abundances approaching 470 ppm, 21 ppm, 1200 ppm, and 800 ppm, respectively (Table 1). Fe (metal) concentrations reach a maximum of 33.6% near the core base (43.4% FeO), decreasing to ~13% (16.4% FeO) just below 2 m depth, at which point concentrations step down to 8–9% (10–11% FeO) in the uppermost 2 m of the core (Figure 4a) indicating a diminished hydrothermal influence upcore. Fe/Mn ratios (Figure 5a) reflect this trend, decreasing from ~6 at the base of the core (MnO = 7 wt.%) to ~3 in the top 2 m of the core (MnO = 3 wt.%), consonant with proportions more typical of Cenozoic pelagic clays elsewhere in the Pacific [*Lyle et al.*, 1986; *Marchig and Erzinger*, 1986; *Kyte et al.*, 1993; *Ziegler and Murray*, 2007]. Because of the small number of samples (n = 26) relative to variables (i.e., elements; n = 26) in our data set, multivariate (factor) analysis was not performed to isolate multiple components; rather, emphasis is placed here on elemental correlations and ratios within the core, using known partitioning behaviors of elements in pelagic clays [e.g., *Kyte et al.*, 1993; *Ziegler and Murray*, 2007].

[13] Elements concentrated in the terrigenous detrital component of pelagic clays [e.g., *Kyte et al.*, 1993; *Dickens and Owen*, 1995; *Ziegler and Murray*, 2007; *Ziegler et al.*, 2007] include Al, Ti (not reported here), Th, Cs, Ta and to a lesser extent Cr, all of which reach greatest abundances in the upper (top 2 m) of the core (Table 1). Al increases systematically from base to top (Figures 4a, 4b, 5b, and 6). Al and Fe (Figures 4a and 5b) in particular show an inverse relationship in this data set, with a crossover point in abundance ratios at about 2 mbsf, implying a change from dominantly hydrothermal sedimentation (~13:1 Fe/Al) lower in the core, to a ~1:1 mix of chemically identified hydrothermal and detrital components at the core top [*Dickens and Owen*, 1995]. Proportions of Fe relative to Al and Mn (Figure 5b) are consistent with a mid-ocean

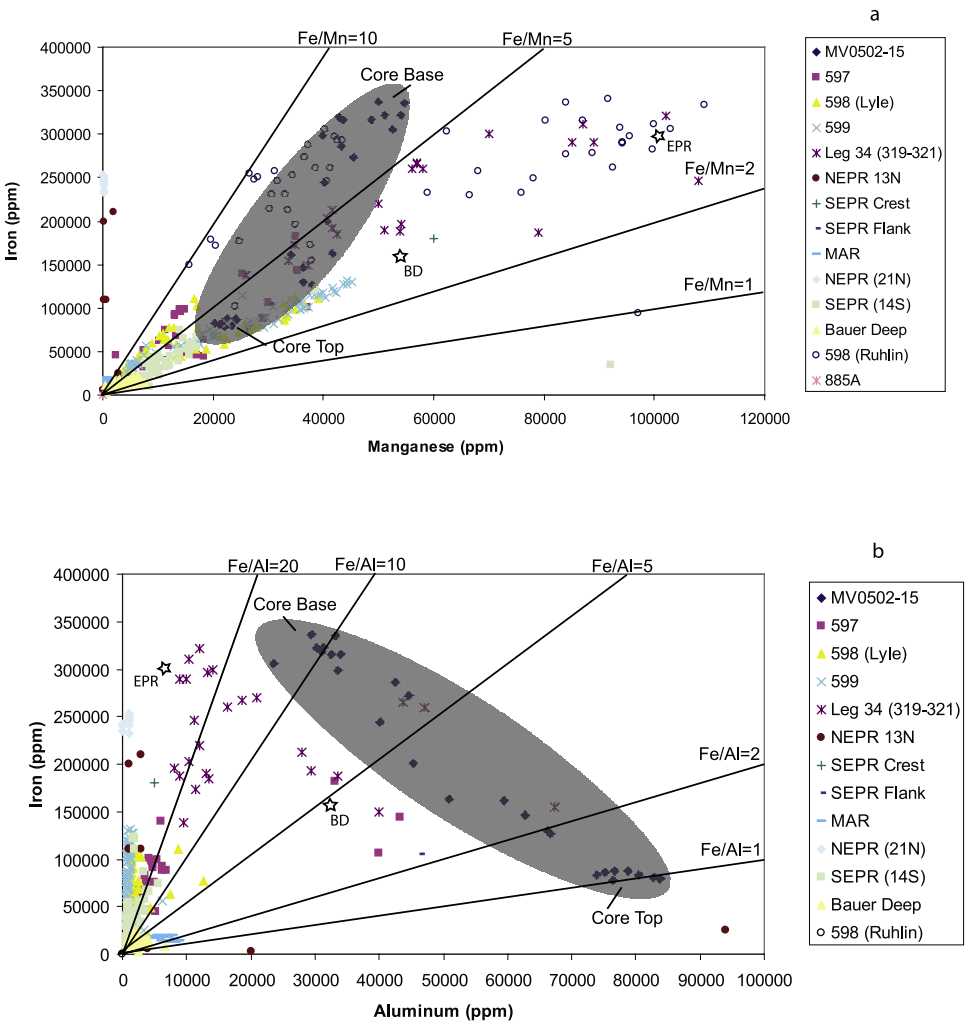

Figure 5. Fe versus Mn and Fe versus Al (in ppm) in MV0502-15JC. Fe/Mn (a) and Fe/Al (b) ratios are distinct between core top and bottom, spanning a range of compositions that overlap data from other marine hydrothermal sediments (see text). Additional data from the following sources: DSDP Sites 597–599 [*Lyle et al.*, 1986]; DSDP Site 319–321 [*Dymond et al.*, 1976]; Mid-Atlantic Ridge Near Totem vent site at 13°N [*German et al.*, 2002]; DSDP Sites 37–39 [*Dymond et al.*, 1973]; DSDP Site 316 and 343 [*Chavagnac et al.*, 2005]; Mid-Atlantic Ridge OBS vent field at 21°N [*German et al.*, 1999]; East Pacific Rise transect at 14°S [*Dunk and Mills*, 2006]; Bauer Deep [*Sayles et al.*, 1975] and DSDP Site 598 [*Ruhlin and Owen*, 1986]. Star symbols are average values for EPR and Bauer Deep metalliferous sediment [*Heath and Dymond*, 1973].

ridge hydrothermal environment for the core base [*Mills and Elderfield*, 1995]. Other elements show more complex behavior: Cr doubles in abundance above 2 mbsf in the core (Table 1), while Ba shows high abundances both at the core base (decreasing through the middle section of the core) and in the uppermost 2 m (>1000 ppm; Table 1).

[14] An Al-Fe-Mn ternary diagram (Figure 6) reinforces the evidence for changing proportions upcore between hydrothermally dominated (Fe-rich) and detrital-dominated (Al-rich) components. Using the core base composition as an end-member for the hydrothermal component, and average upper continental crust (UCC = PAAS; Figure 6) for the end-member detrital component in Fe-Al-Mn space, a mixing trend can be calculated that shows the core top (above 2 m) to be approximately 40% hydrothermal: 60% detrital component with respect to these elements. This estimate does not take into account the percentage authigenic-hydrogenous component, acquired post-deposition by pelagic clays [*Ziegler and Murray*, 2007], which is best factored out using multivariate analysis.

[15] A key indicator of the authigenic signal in pelagic clays is Co [e.g., *Zhou and Kyte*, 1992; *Kyte et al.*, 1993], which is poorly correlated with Fe in our data set. Co tends to be concentrated in pelagic clays as an inverse function of sedimentation rate [*Kadko*, 1985]. Co exhibits maximum variation below 2 mbsf in MV0502-15JC, increasing from

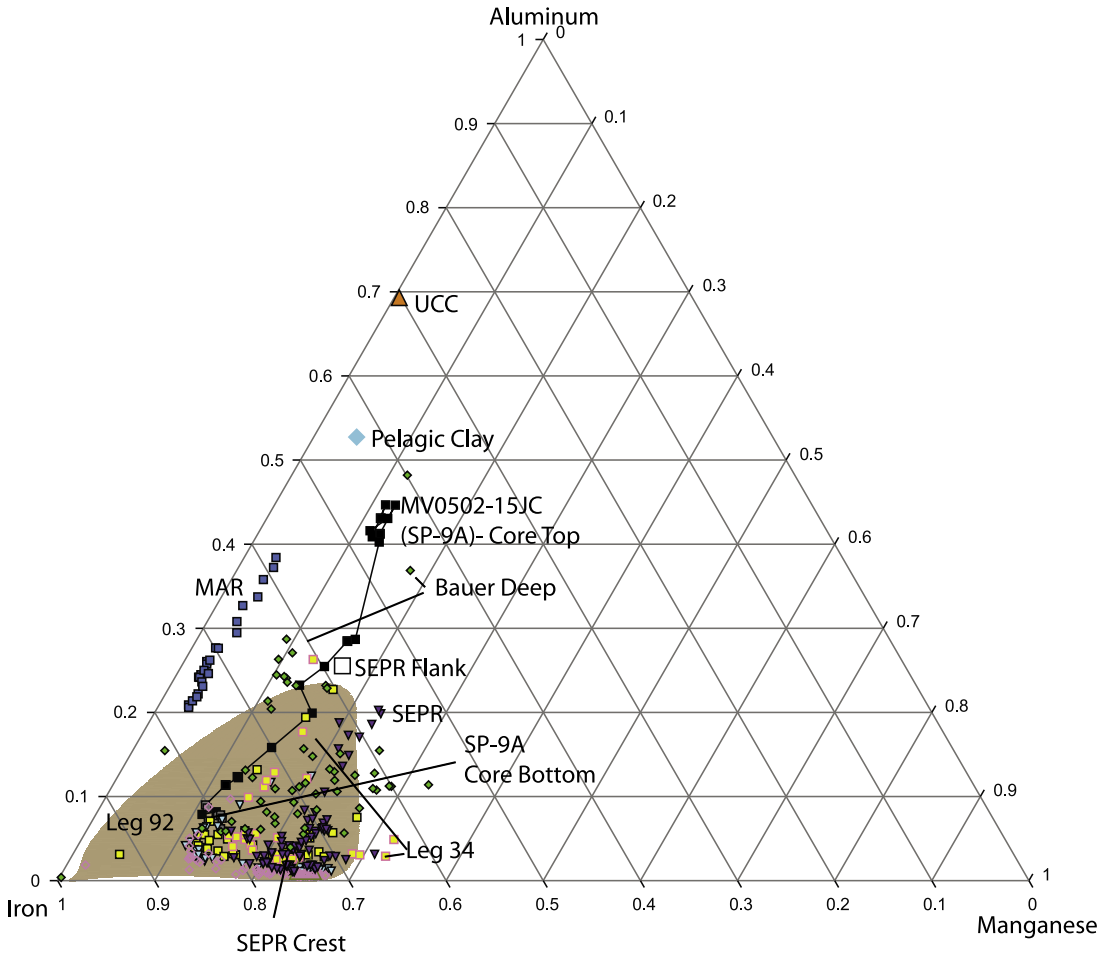

Figure 6. Al-Fe-Mn ternary plot for core MV0502-15JC. Fe is here used as a proxy for the hydrothermal component, and Al as a proxy for the continental detrital (UCC) component. The modern core top appears to be a ~1:1 mix of hydrothermal (Fe-rich) material and terrigenous detrital (Al-rich), while the core base reflects a nearly undiluted (> 95%) hydrothermal signal (see text). Additional data from the following sources: DSDP Sites 597–599 (*Lyle et al.*, 1986); DSDP Site 319–321 [*Dymond et al.*, 1976]; Mid-Atlantic Ridge Near Totem vent site at 13°N [*German et al.*, 2002]; DSDP Sites 37–39 [*Dymond et al.*, 1973]; DSDP Site 316 and 343 [*Chavagnac et al.*, 2005]; Mid-Atlantic Ridge OBS vent field at 21°N [*German et al.*, 1999]; East Pacific Rise transect at 14°S [*Dunk and Mills*, 2006]; Bauer Deep [*Sayles et al.*, 1975; *Heath and Dymond*, 1973] and DSDP Site 598 [*Ruhlin and Owen*, 1986]. UCC and pelagic clay from *Taylor and McLennan* [1985].

200 ppm at the base to 500 ppm at 343 mbsf, then decreasing again to ~300 ppm at the core top (Figure 7 and Table 1). This pattern is consistent with decreasing sedimentation rates upcore (as indicated by the fish tooth stratigraphy), with a sharp break occurring at about 3.5 mbsf (~25 Ma) and another at 2 mbsf (~20 Ma). Below this interval, Co abundances are strongly anti-correlated with Fe (Figure 4a), but well-correlated above 2 mbsf (Figures 4a and 7). This is likely the consequence of an Fe-dominated hydrothermal flux tapering off upcore, with the upper 2 m recording a relative increase in terrigenous flux (Figures 4a, 4b, and 6). A plot of Mn versus Co shows the same trend, demonstrating that both Fe and Mn are strongly partitioned into a hydrothermally sourced component below 2 m, but showing (in particular Mn) a more hydrogenous/authigenic character above this interval in concert with Co, similar to trends observed in other Pacific pelagic clays [*Kyte et al.*, 1993].

[16] Rare earth elements (La through Lu) are uniformly enriched relative to average upper crust (PAAS) in MV0502-15JC (Figures 7 and 8), showing greatest concentrations at depths below 2 mbsf (e.g., max La = 410 ppm at 3.6 mbsf; Figure 7). Such high rare earth element (REE) abundances are typical of distributions associated with marine distal hydrothermal sediments [e.g., *Ruhlin and Owen*, 1986; *Barrett and Jarvis*, 1988; *Dickens and Owen*, 1995]. Above 2 mbsf, REE concentrations are significantly lower (~100–150 ppm La) and relatively constant (Figure 7), similar to abundances reported in Pacific pelagic clays [e.g., *Kyte et al.*, 1993]. REE abundances (except Ce)

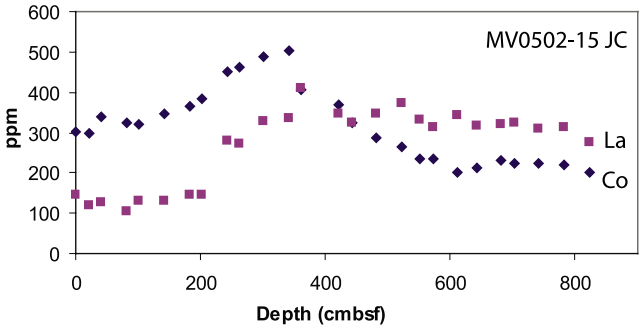

Figure 7. Bulk INAA Co (ppm) and La (ppm) versus Depth in MV0502-15JC. Co abundances increase rapidly (200 to 500 ppm) between 6 mbsf (29.5 Ma) and 3.5 mbsf (26 Ma), consistent with decreasing sedimentation rates over this interval. Maximum Co, recorded between 3.5 mbsf (26 Ma) and 2 mbsf (22.5 Ma), is followed by a slight decrease between 2 mbsf (22.5 Ma) and the core top (300 ppm), where the terrigenous flux appears to dominate. La abundances increase ~50% upcore to a maximum (La = ~400 ppm) at 3.63 mbsf, in concert with other REE. Lower abundances (<150 ppm La) are recorded in the upper 2 m of the core. These trends are typical of "distal" (off-ridge crest) hydrothermal deposits in the marine record (see text).

are tightly correlated throughout the core, showing a systematic increase from the base of the core to their maximum at 3.6 mbsf (Figure 7). Sc, U, Hf and Mo also show correlation with REE (e.g., Sc/Eu, r = 0.95; U/La, r = 0.89; Mo/La, r = 0.84), with Sc/U ratios particularly invariant above (~20) and below (~40) 2 m in the core (Table 1). Hf/Sm ratios also jump to higher values for the upper 2 m of the core, consistent perhaps with an Hf-rich phase (e.g., zircon) dominating more of the Hf budget, as would be expected for loess-like (eolian) material derived from predominantly granitic upper crust [*Taylor and McLennan*, 1985].

[17] Rare earth element abundances in marine sediment are commonly normalized to a shale standard (i.e., PAAS, or Post-Archean Australian Shale), which reveals any departure in the REE pattern from a typical upper crustal signature [*McLennan*, 1989]. The shale-normalized REE patterns in MV0502-15JC (Figure 8) show two distinct REE groupings. Above 2 mbsf, the core has a fairly flat shale-normalized REE pattern typical of an upper continental crust signature (=1 on this plot), although REE abundances are still elevated (~2×) above average crustal values (Figure 8). A small negative Ce-anomaly reveals the presence of a minor scavenged seawater REE component in this part of the core [*Ruhlin and Owen*, 1986]. Below 2 mbsf, REE patterns diverge significantly from the average shale REE pattern, recording large negative cerium anomalies more typical of seawater (Figure 8), and elevated REE concentrations well above average crustal values (LREE > 10× PAAS). Such patterns in marine sediments reflect the scavenging properties of ferromanganese oxide particles associated with hydrothermal plumes [*German et al.*, 1990], and are typical of hydrothermal sediments deposited close to vents as well as pelagic clays deposited at extremely low sedimentation rates far from vent sources [*Ruhlin and Owen*, 1986; *German et al.*, 1990; *Dickens and Owen*,

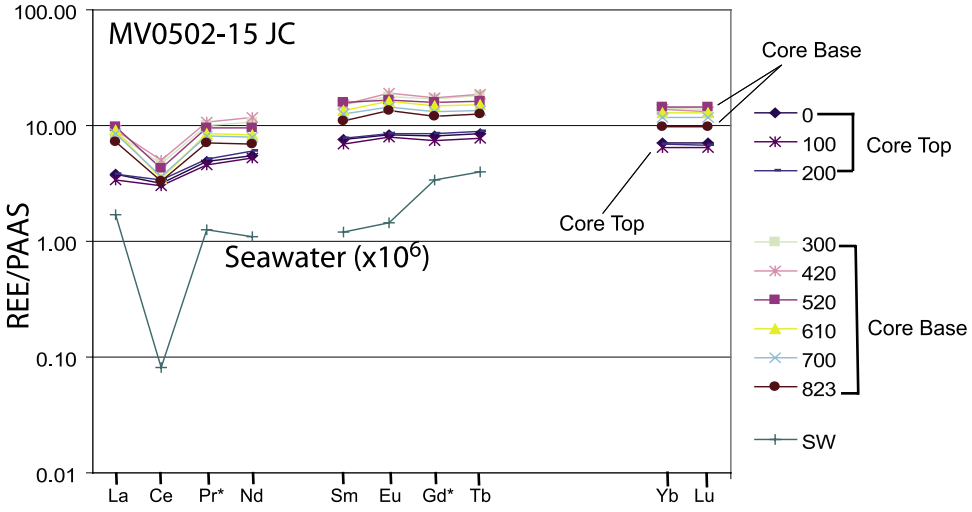

Figure 8. PAAS [Post-Archean Australian Shale from *Taylor and McLennan*, 1985] normalized bulk INAA REE patterns in MV0502-15JC. Seawater pattern (×10^6) for reference [*Piepgras and Jacobsen*, 1992]. The "low" REE group (5–10× crustal abundances) with small Ce anomalies represents the core top (0–2 mbsf), and has the most "shale"-like (flat) patterns. The most REE-enriched samples (>10× crustal abundances), with large Ce anomalies, represent metalliferous clays below 2 mbsf. The two lowermost samples (700 & 823) also have a slight positive Eu anomaly compared to other samples. Pr* and Gd* values were calculated by interpolation from PAAS-normalized patterns as follows: $Pr^*_n = La_n^{1/3} \times Nd_n^{2/3}$ and $Gd^*_n = Sm_n^{1/3} \times Tb_n^{2/3}$.

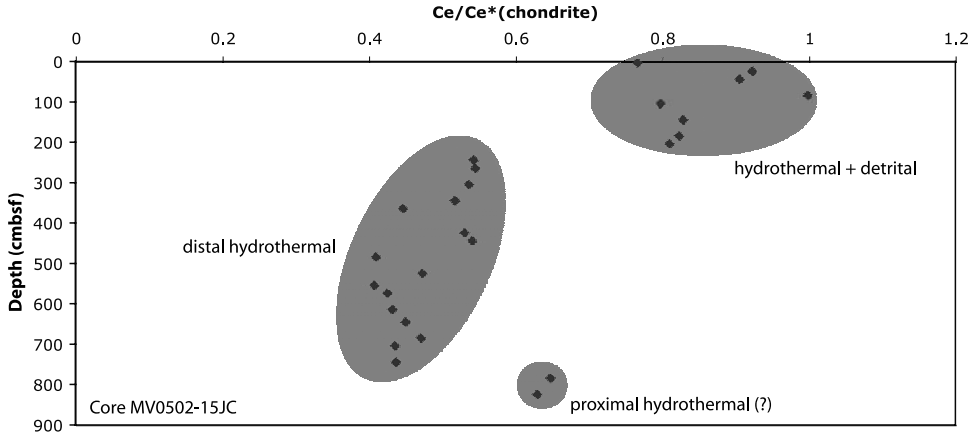

Figure 9. Bulk INAA Ce/Ce* (referenced to chondrite) versus Depth in core MV0502-15JC ($Ce^*_n = La_n^{4/5} \times Sm_n^{1/5}$ using chondritic values; Table 1). Three groups are distinguished that correlate to REE patterns: (1) samples with small cerium anomalies (approaching values of 1 relative to chondrite), these characterize the upper part of the core above 2 mbsf, and are typical of a more shale-dominated signature (i.e., average upper crust); (2) two samples at the base of the core with a Ce anomaly of ~ 0.6, these carry the slight positive Eu anomaly; and (3) samples with a Ce anomaly of $\sim 0.4-0.5$, typical of distal hydrothermal deposits [*Ruhlin and Owen*, 1986; *Dickens and Owen*, 1995]. The negative Ce anomaly indicates primary source of scavenged REE is seawater.

1995; *Ziegler and Murray*, 2007]. The very base of the core has a minor positive anomaly (Eu/Eu* = 1.2–1.3) that may indicate an additional component (Figure 8) not present upcore; such anomalies have been identified in hydrothermal fluids at their vent source, as well as in direct precipitates from ridge crest vents, and are derivative of leached mineral phases (i.e., feldspar) in basalt [*Michard et al.*, 1983; *German et al.*, 1997; *Klinkhammer et al.*, 1994]. Some quantification (see below) of the scavenged seawater component can be modeled in terms of the Ce-anomaly (Ce/Ce*; Figure 9), which shows the same three distinct groupings in MV0502-15JC noted above.

3.3. Radiogenic Isotopic Composition of the Extracted Detrital Component

[18] The Nd isotopic composition of the extracted (<38 micron) detrital component varies between ε_{Nd} of −4.6 and −7.7, with the least negative value (−4.6) at the core base (8.23 mbsf), and the most negative values (−7.7) just below 2 mbsf (Table 3). Four intervals from the upper 2 m of the core are clustered around intermediate values of −6.0 to −6.8 (average −6.4). Such values are typical of an evolved, upper crustal source for Nd [*Taylor and McLennan*, 1985], although a remnant Pacific seawater-derived component cannot be ruled out either; detrital rare Earth element (REE)

Table 3. TIMS Nd-Sr Isotopic Composition of Terrigenous Extract for Piston Core MV0502-15JC[a]

Depth, cmbsf	$^{87}Sr/^{86}Sr$[b]	2SE±[c]	$^{143}Nd/^{144}Nd$[d]	2SE±[c]	Corrected[e]	ε_{Nd}[f]
0–2	0.703391	0.000017	0.512255	0.000009	0.512292	−6.75
22–24	0.713317	0.000024	0.512291	0.000010	0.512328	−6.05
102–104	0.712174	0.000017	0.512259	0.000009	0.512296	−6.67
182–184	0.711550	0.000016	0.512297	0.000009	0.512334	−5.93
262–264	0.717440	0.000012	0.512225	0.000010	0.512262	−7.33
342–344	0.717338	0.000013	0.512206	0.000010	0.512243	−7.71
382–384	0.713846	0.000018	0.512272	0.000010	0.512309	−6.42
442–444	0.713860	0.000014	0.512217	0.000010	0.512254	−7.49
552–554	0.711950	0.000015	0.512269	0.000009	0.512306	−6.48
612–614	0.713012	0.000015	0.512283	0.000010	0.512320	−6.20
702–704	0.711395	0.000016	0.512284	0.000010	0.512321	−6.18
822–824	0.708399	0.000017	0.512366	0.000010	0.512403	−4.58
NZ loess	0.710459	0.000018	0.512316	0.000010	0.512353	−5.56

[a]NBS 987 measured at Michigan was $^{87}Sr/^{86}Sr = 0.710234 \pm 14$ (n = 67), late 2006 La Jolla Nd measured at Michigan was $^{143}Nd/^{144}Nd = 0.511813 \pm 8$ (n = 20), late 2006.
[b]Normalized to $^{86}Sr/^{88}Sr = 0.1194$.
[c]Internal (measured) error.
[d]Normalized to $^{146}Nd/^{144}Nd = 0.7219$.
[e]Corrected to La Jolla value of $^{143}Nd/^{144}Nd = 0.511850$ (old Michigan value).
[f]$\varepsilon_{Nd} = 10^4[(^{143}Nd/^{144}Nd_{sample})/(^{143}Nd/^{144}Nd_{chur}) - 1]$, where $^{143}Nd/^{144}Nd_{chur} = 0.512638$.

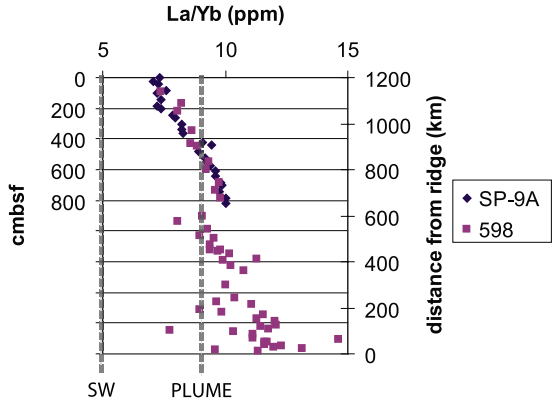

Figure 10. Bulk INAA La/Yb (ppm) versus Depth, core MV0502-15JC. La/Yb decreases systematically upcore from the base (with a break in the trend at ~ 2 mbsf), implying increasing distance from hydrothermal sources (see text), similar to the trend identified by *Ruhlin and Owen* [1986] at DSDP Site 598. This comparison allows for a crude estimate of distance (~450–900 km) from a potential ridge crest source for core site SP-9A at ~ 31 Ma (see text). SW = seawater [*McLennan*, 1989]; PLUME = hydrothermal plume particulates [*Sherrell et al.*, 1999]. These trends indicate that even at the top of the core, REE budgets contain a significant seawater (hydrogenous) component.

patterns (see below) suggest that any seawater component is not significant. These Nd isotopic values are less negative than pelagic clay extracts from surface sediments in the central North Pacific ($\varepsilon_{Nd} = -10$), which are indicative of late Cenozoic Asian dust sources [*Nakai et al.*, 1993; *Jones et al.*, 1994; *Pettke et al.*, 2000, 2002; *Stancin et al.*, 2006]. Sr isotopic compositions are least radiogenic at the core base ($^{87}Sr/^{86}Sr = 0.7084$), increasing upcore to a maximum $^{87}Sr/^{86}Sr$ of 0.7174 just below 2 mbsf, in concert with Nd. Again, a seawater component could be influencing these values, although the detrital fractions are much more radiogenic (for Sr) than contemporary seawater at a given age/interval [*McArthur et al.*, 2001]. The uppermost 2 m of the core trend toward more intermediate values, from $^{87}Sr/^{86}Sr = 0.7116$ (1.83 mbsf) to 0.7134 (core top). A sample of Quaternary loess collected from the Canterbury Plain of the New Zealand, South Island (sub-38 micron fraction extract) has $\varepsilon_{Nd} = -5.6$ and $^{87}Sr/^{86}Sr = 0.710459$, slightly more radiogenic (less negative) for Nd and less radiogenic for Sr than the upper part of the core (average = −6.4; 0.7126); this comparison suggests a slightly older crustal provenance for the core material.

4. Discussion

4.1. REE Geochemical Constraints on Hydrothermal Sources

[19] Hydrothermal venting of the ocean floor, particularly along spreading ridges, releases reduced Fe and other dissolved metals into the water column; as the Fe reacts with dissolved O_2 and precipitates, it efficiently incorporates elements forming oxyanions (e.g., As, Sb, V) in seawater [e.g., *Michard et al.*, 1983; *German et al.*, 1990, 1999; *Rudnicki and Elderfield*, 1993; *Mills and Elderfield*, 1993, 1995]. Once precipitated, the Fe oxyhydroxides also begin scavenging elements, particularly the rare earth elements (REE), from seawater. This scavenging occurs within the hydrothermal plume, but also continues long after deposition as long as the Fe oxides remain near the seawater-sediment interface; consequently, hydrothermal precipitate REE contents can be enriched relative to REE concentrations in seawater by several orders of magnitude, and over vent fluid REE concentrations by at least a factor of 10 [e.g., *Ruhlin and Owen*, 1986; *Olivarez and Owen*, 1989a; *German et al.*, 1990, 1993; *Dickens and Owen*, 1995].

[20] Studies of marine sediments by *Ruhlin and Owen* [1986], *Barrett and Jarvis* [1988], *Owen and Olivarez* [1988] and *Olivarez and Owen* [1989a], among others, have shown that distal, hydrothermally influenced sediments far from mid-ocean ridge vent sources are the most highly enriched in total REE, while proximal (i.e., younger) hydrothermal precipitates are more enriched in LREE relative to HREE, leading to higher LREE/HREE ratios closer to vent sources. The top 2 m of core MV0502-15JC (Figure 10) has the lowest La/Yb ratio (~7), with LREE/HREE fractionation increasing systematically down core to values of around 10 (a small jump in values occurring at ~2 mbsf and also at ~4 mbsf). This not only suggests a more proximal hydrothermal influence for the lower part of the core (deposited at higher sedimentation rates), but because the trend is continuous with core depth and age, it also implies either steady movement away from, or diminishing input from, vent sources with time [*Ruhlin and Owen*, 1986]. La/Yb ratios in MV0502-15JC (Figure 10) are compared with another South Pacific pelagic clay core (DSDP Site 598; Figure 1), which has values 'calibrated' by distance from ridge. This comparison suggests that MV0502-15JC records hydrothermal sedimentation approximately ~600 km to ~1200 km down-plume from a potential ridge source. While such a comparison does not take into account variables such as sedimentation rate, depth of burial, ocean currents, plume production rates or particle size distribution [*Dickens and Owen*, 1995], these inferred distances are nonetheless consistent with the presence of another 16 m of metalliferous sediment imaged between the base of the core (8.35 mbsf) and ~55 million year old basement (~24 mbsf).

[21] REE/Fe ratios also potentially provide some indication of the relative distance at which marine hydrothermal sediments are deposited from ocean ridge vent sources [*Olivarez and Owen*, 1989a]. While the distal portions of hydrothermal plume systems scavenge REE from seawater as a function of suspension time and particle size [*German et al.*, 1990], Fe is more concentrated in hydrothermal precipitates deposited closer to the source; thus, the lowest REE/Fe ratios at the core base (~8 to ~6 mbsf) in MV0502-15JC are most consistent with more proximal hydrothermal sources (Figure 11), in concert with the La/Yb data, Ce- and Eu-anomalies discussed above. REE/Fe ratios increase steadily upcore from ~6 mbsf to about 2 mbsf, above which a terrigenous component appears

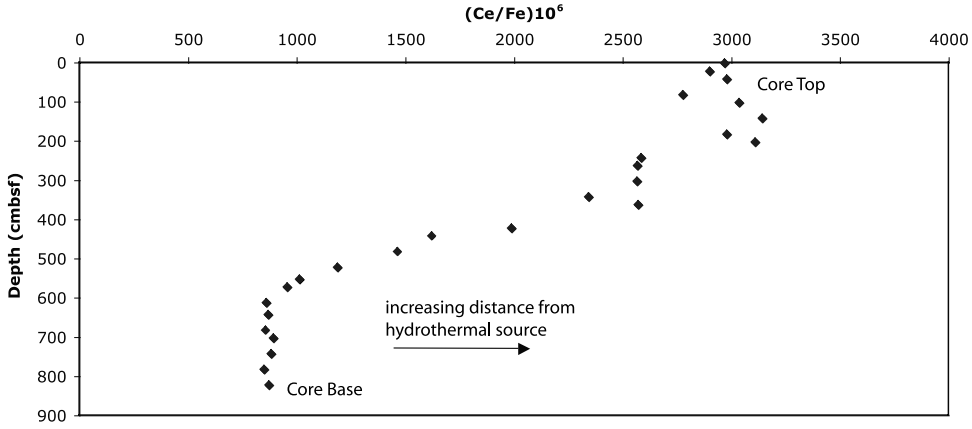

Figure 11. Bulk INAA REE (Ce/Fe) versus Depth for core MV0502-15JC. Such ratios can also be considered a rough proxy for relative distance from an ocean ridge hydrothermal vent source environment [*Olivarez and Owen*, 1989a]. The low ratios at the base of the core suggest more proximal hydrothermal sources (ridge crest), with distal hydrothermal influence (ridge flank) diminishing steadily upcore to a more terrigenous-dominated core top (see text).

to combine with a background hydrothermal component in roughly constant proportions to the core top, as indicated by Fe/Al ratios. These coherent REE/Fe variation patterns are similar to those displayed by other Pacific pelagic cores carrying variable contributions of a hydrothermal component [*Kyte et al.*, 1993]. With the caveat that elevated REE abundances in pelagic sediments are 1) an inverse function of sedimentation rate and, 2) proportional to exposure age [i.e., authigenic control; *Ziegler and Murray*, 2007], a further constraint on distance from hydrothermal sources can be computed using these data. Table 4 shows a comparison of MV0502-15JC REE/Fe ratios with DSDP Site 598 (Figure 1). This drill site, northeast of site SP-9A, captures a complete 16 Ma late Cenozoic hydrothermal sedimentation history, referenced to distance from spreading ridge [*Ruhlin and Owen*, 1986; *Olivarez and Owen*, 1989a]. Comparisons of REE/Fe data suggests that the base of the MV0502-15JC core could have been ~500 to 900 km from a ridge (or, more specifically, the source of the hydrothermal flux), in agreement with the La/Yb data described above (Figure 10). This comparison is made assuming similar sedimentation rates and largely carbonate-free sections [*Dickens and Owen*, 1995].

4.2. Origin of the Hydrothermal Component: Regional Comparisons and Tectonic Setting

[22] The high amount of iron oxide that characterizes the lower part of core MV0502-15JC (Table 1 and Figures 4, 5, and 6) is unusual in seafloor hydrothermal sediments deposited away from vent sites because biogenic (e.g., calcium carbonate) or terrigenous components typically dilute the signal. There are, however, both modern and ancient analogues. For example, the modern day Bauer Deep, a failed rift between the EPR and Galapagos Rise [*Mammerickx*, 1992; *Devey et al.*, 1997], sits at a water depth of 4–5 km [*Sayles et al.*, 1975], well below the CCD. Sediment in that basin is dominated by distal hydrothermal material, and yet has an Fe content between 12 and 28 wt.% [*Dymond et al.*, 1973], about the same range as that recorded in the bottom ~6 m of MV0502-15JC. Moreover, hydrothermal material has accumulated at both sites at rates of up to 2 mm/ka [*Sayles et al.*, 1975]. Another (paleo) example is Chinook Trough, a remnant of Late Cretaceous intraplate spreading within the Farallon Plate in the North Pacific. South of the Chinook Trough, at ODP Site 885/886, there is a ~10 Ma record of Late Cretaceous distal hydrothermal sediment deposited below the CCD [*Dickens and Owen*, 1995] Again, bulk Fe concentrations near the base of the sequence range from 23.5% to 32.5%, overlapping those near the base of MV0502-15JC. However, estimated linear sedimentation rates for Late Cretaceous distal hydrothermal sediment at Chinook Trough [~0. 65 mm/ka; *Ingram*, 1996; *Dickens and Owen*, 1995] are lower than our estimates for Oligocene distal hydrothermal sedimentation rates at site SP-9A (~2 mm/ka). The hydrothermal record at Site SP-9A may attest to a specific depositional environment: a deep, open-ocean region near a spreading system. In this way, it received very little dilution from biogenic (i.e., below the CCD) and detrital inputs, consistent with its location within the South Pacific bare zone [*Rea et al.*, 2006].

[23] Chinook Trough may in some ways be analogous to the Adventure Trough [*Cande and Haxby*, 1991], a possible failed rift <2° east of site SP-9A (Figure 1). *Cande and Haxby* [1991] suggested that Adventure Trough had been the site of a propagating rift related to a series of Eocene ridge jumps in the Southwest Pacific at about chron 16 [~36 Ma; *Tebbens and Cande*, 1997]. Little is known about how long, or even whether, the Adventure Trough was an active spreading center; it may never have been [*S. Cande*, personal communication, 2007]. Nonetheless, as noted by *Jordahl et al.* [1998], the Adventure Trough has been a site of mid-plate volcanic activity in the past. By 34 Ma (Chron 13), the locus of rifting became the active Pacific-Farallon spreading center [*Cande and Haxby*, 1991], several hundred kilometers more distant from Site SP-9A (Figure 1). With REE/Fe and La/Yb ratios both suggesting hydrothermal sources between 400 and 900 km away from Site SP-9A at ~31 to 30 Ma, the Adventure Trough and the

Table 4. REE/Fe Comparison Between Piston Core MV0502-15JC and DSDP Site 598

MV0502-15 JC									DSDP Site 598								
cmbsf	La/Fe	Ce/Fe	Nd/Fe	Sm/Fe	Eu/Fe	Tb/Fe	Yb/Fe	Lu/Fe	km from ridge	La/Fe	Ce/Fe	Nd/Fe	Sm/Fe	Eu/Fe	Tb/Fe	Yb/Fe	Lu/Fe
2	1711	2970	2089	498	107	78	233	36	1139	1728	699	1379	380	102	76	235	51
23	1447	2902	1570	417	91	65	204	30	1085	1813	697	1000	381	96	62	220	58
43	1452	2980	1786	422	105	73	200	29	1055	1676	653	1462	353	89	64	208	46
83	1232	2778	1499	351	73	53	162	26	970	1401	436	1030	288	71	49	162	40
103	1643	3036	2152	487	112	76	228	35	912	1380	308	1164	249	68	51	160	35
143	1639	3143	2142	488	108	75	223	34	904	1320	297	870	245	63	46	149	37
183	1631	2980	1879	476	104	68	226	34	832	1298	280	670	225	58	38	139	35
203	1649	3110	2189	498	106	79	224	33	802	1221	218	991	203	56	35	132	28
243	2190	2586	2387	557	127	93	279	42	742	1277	268		186	48	25	131	34
263	2088	2568	2542	535	126	92	263	40	710	1028	203	502	153	42	32	107	24
303	2219	2567	2351	571	134	95	270	41	675	1036	180		149	38	22	106	24
343	2070	2344	2290	540	124	91	252	37	596	831	156		133	34	21	92	22
363	2512	2572	3184	658	158	115	303	45	574	687	0		132	37	20	85	18
423	1722	1989	1877	420	104	72	190	28	540	657	131		106	27	22	71	15
443	1315	1622	1087	305	81	56	139	22	513	566	77		93	24	15	63	12
483	1268	1463	1285	298	82	55	142	21	500	609	123		97	26	17	64	15
523	1299	1189	1068	307	63	43	141	22	474	604	139		96	25	16	64	14
553	1104	1013	988	252	58	39	119	19	453	502	122		81	21	11	51	12
573	992	956	915	223	54	37	105	17	450	465	84	369	79	22	14	50	11
613	1076	860	840	236	56	37	112	17	444	494	119		81	22	19	51	12
643	1006	869	860	219	50	35	105	16	436	460	108		73	19	11	45	11
583	950	857	761	203	49	34	97	15	414	462	90	320	68	19	10	41	11
703	1006	893	781	217	49	32	102	16	404	420	107	247	68	19	12	42	9
743	915	883	759	201	49	33	94	14	385	425	104	363	69	19	10	42	10
783	972	850	783	215	51	34	97	15	363	423	117		69	18	15	39	10
823	899	873	722	199	49	32	90	14	298	354	40	71	56	15	10	35	7
									244	350	81		53	14	8	34	9
									227	363	54	232	58	16	8	38	8
									212	354	57		51	13	10	32	8
									194	323			52	14	10	36	7
									178	288	22	248	49	13	9	29	6
									170	384	75		57	15	7	33	8
									152	327	41	137	49	13	7	29	7
									140	370	54		52	14	7	31	7
									122	376	26	94	57	16	9	31	7
									120	317			49	13	7	28	6
									109	321	61		49	13	6	27	6
									103	356	56		55	14	8	46	7
									95	213			35	10	5	21	4
									85	316	23	209	48	13	8	28	6
									66	210			32	9	4	19	5
									61	444	73	360	56	15	8	30	6
									52	337		212	53	14	7	29	7
									48	333	33	223	53	14	9	28	6
									40	295	44	228	49	13	8	25	6
									36	377	69	239	56	15	8	31	7
									28	294	39	198	47	12	7	25	5
									20	335	81		49	13	6	26	6
									16	121		113	27	7	4	13	3
									9	228	13	185	40	10	5	20	4

Pacific-Farallon spreading center would be leading candidates for potential sources; the Adventure Trough is at the near-end at ~450 km (@31 Ma), and the Pacific-Farallon Ridge at the far end [900 km @ 31 Ma; *Tebbens and Cande*, 1997] of this range. The Pacific-Farallon Ridge, which was active until the Miocene (~20 Ma), when the spreading center shifted to the present-day East Pacific Rise [*Okal and Bergeal*, 1983], might best account for the lithologic and geochemical changes observed at approximately 200 cmbsf in MV0502-15JC, which corresponds to an age of ~20 Ma.

[24] Detailed reconstructions of the southwestern Pacific, the Pacific-Antarctic Ridge, and the East Pacific [*Wells*, 1989; *Stein and Robert*, 1985; *Cande et al.*, 1995; *Maia et al.*, 2005; *Lamarche et al.*, 1997; *Tebbens and Cande*, 1997; *Schellart et al.*, 2006] also indicate that Cenozoic seafloor of the South Pacific experienced numerous ridge jumps creating short-lived oceanic microplates. *Lyle et al.* [1987] and *Olivarez and Owen* [1989b] demonstrated a connection between plate tectonic reorganizations such as ridge jumps, ridge-transform rearrangements, and ridge abandonment with mid plate or circum-Pacific volcanic and hydrothermal activity. Just prior to a regional plate reorganization at 24 Ma [*Lyle et al.*, 1987; *Tebbens and Cande*, 1997], there was active volcanism in the nearby Austral-Cook seamount chain [*Clouard and Bonneville*, 2005], coinciding with the hydrothermal record at site SP-9A. The southern-most

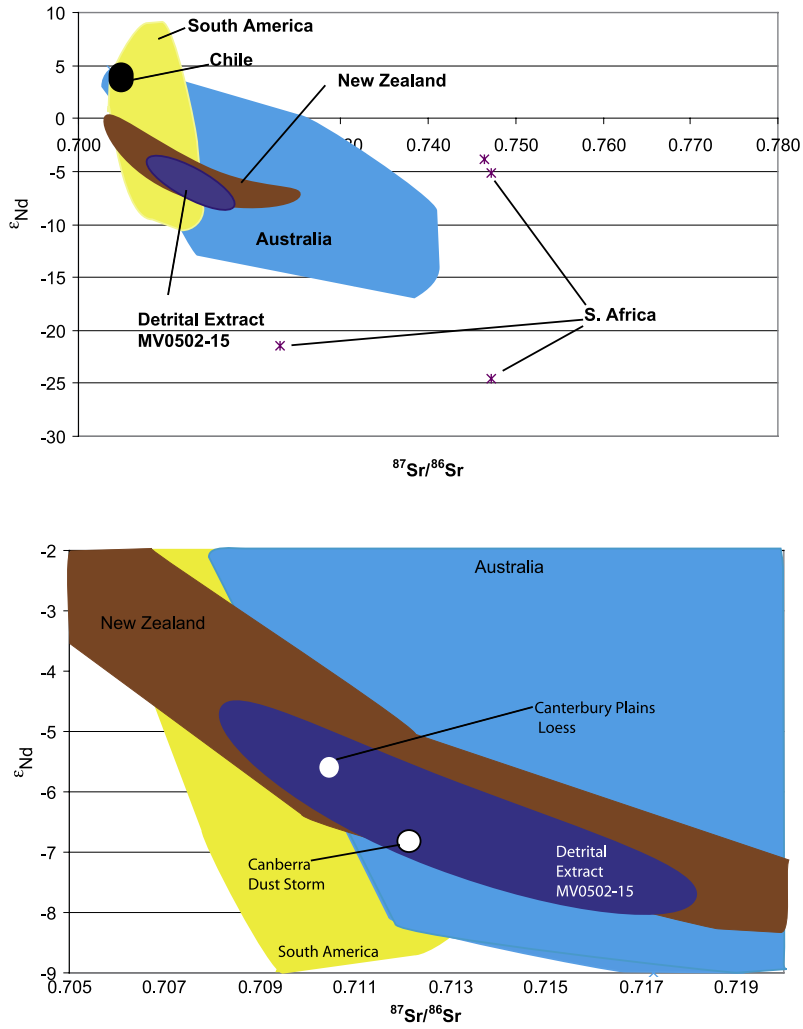

Figure 12. $^{87}Sr/^{86}Sr$ versus ε_{Nd} for southern hemispheric eolian continental loess materials [*Smith et al.*, 2003; *Delmonte et al.*, 2004, *Revel-Rolland et al.*, 2006] and the <38 u extract from MV0502-15JC (Table 3). Despite considerable scatter, values for Australia and NZ appear to be the best match for the detrital component in MV0502-15JC.

Austral-Cook seamount chain is approximately 4 degrees north (450km) of site SP-9A, with the currently active MacDonald seamount the farthest south (Figure 1). *Clouard and Bonneville* [2001, 2005] showed that the present-day Austral-Cook chain overprints much older seamounts ranging in age from 22–39 million years old, just a few hundred km north of the core site. For a precursor to the Austral-Cook seamounts to have produced ~6+ m of hydrothermal sediment at Site SP-9A, the hydrothermal flux to the site should have increased upcore as the plate moved west-northwest; instead, the opposite is observed.

[25] The record of hydrothermal sedimentation preserved in piston core MV0502-15JC appears to be unique within the SW Pacific Basin. *Zhou and Kyte* [1992] examined pelagic clay at DSDP Site 596 (23°51.20′S, 169°39.27′W) in the South Pacific, northwest of SP-9A (Figure 1). At DSDP Site 596, the hydrothermal component does not exceed 10% of the total sediment mass fraction between 31 Ma and the present [*Zhou and Kyte*, 1992], with calculated hydrothermal MAR < 0.5 mg/cm^2/ka over the 31–20 Ma interval; little connection therefore appears to exist between Cenozoic hydrothermal sedimentation in the SPBZ and areas >1000 km to the northwest of it. A second piston core (MV0502-16JC, TUIM-03), taken near MacDonald Seamount just outside the SPBZ [*Rea et al.*, 2006], recovered 10.5 m of hydrothermal sediment and biogenic ooze [*Stancin et al.*, 2007]. Concordant nanofossil and fish teeth ages at the base of this core (~27–28 Ma) reinforce the validity of the Sr fish teeth method used here for dating hydrothermal cores [*Ingram*, 1995; *Snoeckx et al.*, 1995]. These independent records imply that intense Oligocene hydrothermal activity recorded within the SPBZ was regional in extent.

4.3. Origin of the Terrigenous Component in Piston Core MV0502-15JC

[26] Sr and Nd isotopic compositions of the extracted detrital component (Table 4) in MV0502-15JC are plotted

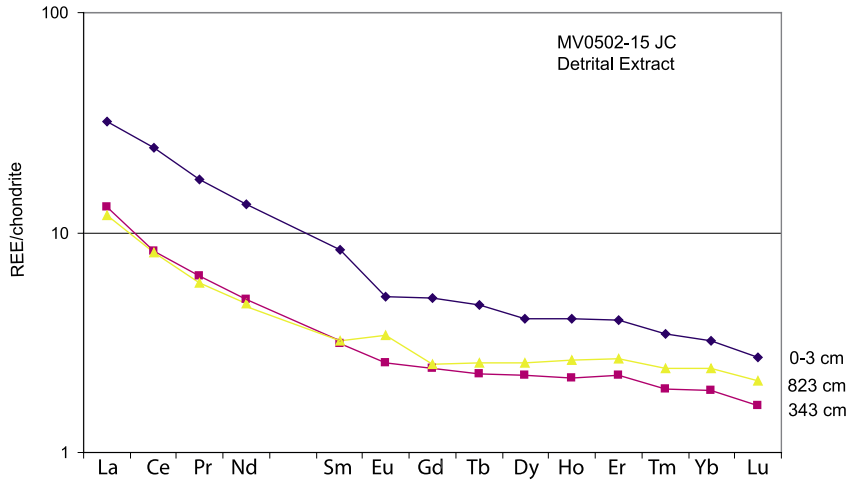

Figure 13. ICP-MS REE data for detrital extract from three intervals in MV0502-15JC. Chondrite-normalized REE patterns for three samples of the <38 micron detrital fraction show decreasing Eu anomalies upcore to a crustal (or loess-like) REE pattern at the core top. The lack of Ce anomalies reflects near-complete removal of the seawater hydrothermal component during the chemical extraction process.

for comparison with potential southern hemisphere eolian dust sources (Figure 12). Most southern hemisphere dust sources appear to have similar Nd-Sr isotopic signatures [*Smith et al.*, 2003; *Delmonte et al.*, 2004, *Revel-Roland et al.*, 2006]. Aside from South Africa and a few other ancient cratonic regions (e.g., W. Australia), there is really no way to distinguish on this basis a specific source of the terrigenous component at such a remote site. The least negative ε_{Nd} value (−4.6) corresponds to the base of the core, as does the least radiogenic Sr ($^{87}Sr/^{86}Sr = 0.7084$), consistent with mixing between a crustal and a more mantle−like isotopic component in the oldest detrital fraction, as hypothesized based on the bulk INAA REE patterns. Chondrite−normalized REE patterns for the < 38 micron detrital fraction show, with the exception of the oldest sample, a dominantly crustal (loess−like) negative Eu anomaly, consistent with the extracted component in the core being eolian in origin (Figure 13).

[27] The Nd−Sr isotopic data are at least consistent with several well−characterized continental source regions in the Southern Hemisphere. Chilean loess has positive Nd values (+3.3 to +4.6) [*Walter et al.*, 2000], unlike the MV0502−15 detrital extract (Figure 12), which would appear to rule out South American sources. However, Argentine loess [8.3 to −6.4; *Gallet et al.*, 1998; *Delmonte et al.*, 2004] overlaps in Nd-Sr isotopic space (Figure 12), though it is not favorably situated with respect to zonal wind patterns for dust delivery to the SW Pacific Basin [*Rea*, 1994]. Southeastern Australia has a large Nd-Sr range [*Delmonte et al.*, 2004] that overlaps the isotopic composition of the MV0502-15 detrital component (Figure 12). A modern dust storm in Canberra plots in the midst of the MV0502-15 core extract data [*Revel-Roland et al.*, 2006]. Loess from the South Island of New Zealand, both the Banks Peninsula [*Taylor et al.*, 1983] as well as Canterbury Plains (sample provided by P. Tonkin), also occupies the same isotopic space (Figure 12). As noted by *Revel-Roland et al.* [2006], these Southern Hemisphere continental sources are largely indistinguishable from dust preserved in Antarctic ice cores, testifying to the widespread dispersal of a highly homogenized dust signal over a large region of the South Pacific during the late Cenozoic.

[28] It is likely that the core site would have received increasing amounts of dust during the late Cenozoic as Australia migrated north into a drier climate belt, more accessible to areas downwind [*Stein and Robert*, 1985]. *Stein and Robert* [1985] determined that in the Mid Miocene (∼12.5 Ma) there was an increase in illite in a drill core at Lord Howe Rise (Tasman Sea), indicating a shift to a drier climate. The shift to a more arid climate should lead theoretically to more dust being available for transport to remote downwind sites [*Rea*, 1994]. Finally, as the site migrated with the Pacific plate W-NW, Australia and NZ would have been increasingly more proximal dust sources. New Zealand and its abundant loess deposits would have become a tectonically uplifted and glaciated source by ∼6 Ma or even earlier [*Lu et al.*, 2005], likely contributing more to the mix. Isotopically, Australia and New Zealand dust sources cannot be distinguished from each other at such a distal location in the remote South Pacific.

5. Conclusions

[29] Core MV0502-15JC (Site SP-9A 31.75°S, 143.5°W) retains a record of intense early Oligocene hydrothermal activity that may be related to ridge jump/ridge propagation events (Adventure Trough), seamount volcanic activity (MacDonald Seamount precursors), or seafloor spreading in this region of the SW Pacific basin (Pacific-Farallon Ridge). The hydrothermal flux (2 mm/ka LSR) decreases exponentially between 31 Ma and the present, suggesting tectonic migration away from a spreading center. Such a source would have been largely extinguished by ∼20 Ma. The Pacific-Farallon Ridge best fits these criteria. An additional ∼16 m of >31 Ma (<55 Ma) sediment at this site, not recovered by the core studied here, may imply an even longer, more complex record of hydrothermal activity relat-

ing either to Eocene plate tectonic reorganization or spreading along the Pacific-Farallon Ridge. Reduced sedimentation rates ~19 Ma to the present (<0.05 mm/ka LSR) reflect a significant reduction of the hydrothermal component relative to the terrigenous component, which is interpreted to be eolian dust of Australian/New Zealand derivation. Further exploration of Cenozoic hydrothermal activity in the South Pacific "bare zone", an anomalous region lacking pelagic sediment cover, will benefit from high-resolution dating of piston cores by Sr isotope fish teeth stratigraphy.

[30] **Acknowledgments.** We thank Leah Minc of Oregon State University for the neutron activation analysis, and Marcus Johnson (RIGL) for analytical help at the University of Michigan. Eric Portenga was invaluable in helping with sample preparation. Steve Cande was very kind in answering questions and providing seafloor age maps for the R/V Melville cruise. We are indebted to the South Pacific LAtitudinal Transect (SPLAT) crew and science party on the R/V Melville, without whom none of this work would have been possible. A special thank you to the shipboard core techs, who accomplished amazing things under extreme weather conditions. The SPLAT cruise was supported by NSF grant OCE-0240924 to the University of Michigan, and OCE-0240906 to Boise State University. Many thanks to G. Dickens, R. Murray and an anonymous reviewer - their help is gratefully acknowledged.

References

Barrett, T. J., and I. Jarvis (1988), Rare-earth element geochemistry of metalliferous sediments from the DSDP leg 92: The East Pacific Rise transect, *Chem. Geol.*, *67*, 243–259.

Cande, S. C., and W. F. Haxby (1991), Eocene propagating rifts in the Southwest Pacific and their conjugate features on the Nazca Plate, *J. Geophys. Res.*, *96*(B12), 19,609–19,622.

Cande, S. C., C. A. Raymond, J. Stock, and W. F. Haxby (1995), Geophysics of the Pitman fracture zone and Pacific-Antarctic plate motions during the Cenozoic, *Science*, *270*(5238), 947–953.

Chavagnac, V., C. R. German, J. A. Milton, and M. R. Palmer (2005), Sources of REE in sediment cores from the Rainbow vent site (36° 14′N, MAR), *Chem. Geol.*, *216*, 329–352.

Clouard, V., and A. Bonneville (2001), How many Pacific hotspots are fed by deep-mantle plumes?, *Geology*, *29*(8), 695–698.

Clouard, V., and A. Bonneville (2005), Ages of seamounts, islands, and plateau on the Pacific plate, *Geol. Soc. Am. Spec. Pap.*, *388*, 71–90.

Delmonte, B., I. Basile-Doelsch, J.-R. Petit, V. Maggi, V. Revel-Rolland, M. Michard, E. Jagoutz, and F. Grousset (2004), Comparing the Epica and Vostok dust records during the last 220,000 years: Stratigraphical correlation and provenance in glacial periods, *Earth Sci. Rev.*, *66*, 63–87.

Devey, C. W., et al. (1997), The Foundation Seamount chain: A first survey and sampling, *Mar. Geol.*, *137*, 191–200.

Dickens, G. R., and R. M. Owen (1995), Chinook Trough rifting and hydrothermal deposition at Sites 885 and 886, In Rea, D. K., Basov, I. A., Scholl, D. W., Allan, J. F. (eds), *Proc. Ocean Drill. Program Sci. Results*, *145*, 413–425.

Doyle, P. S., and W. R. Riedel (1979), Cretaceous to Neogene ichthyoliths in a giant piston core from the central North Pacific, *Micropaleontology*, *25*, 337–364.

Dunk, R. M., and R. A. Mills (2006), The impact of oxic alteration on plume-derived transition metals in ridge flank sediments from the East Pacific Rise, *Mar. Geol.*, *229*, 133–157.

Dymond, J., J. B. Corliss, G. R. Heath, C. W. Field, E. J. Dasch, and H. H. Veeh (1973), Origin of metalliferous sediments from the Pacific Ocean, *Geol. Soc. Am. Bull.*, *84*, 3355–3372.

Dymond, J., J. B. Corliss, and R. Seillinger (1976), Chemical composition and metal accumulation rates of metalliferous sedments from sites 319, 320B and 321, *in* Initial reports of the Deep Sea Drilling Project, Vol. 34; Washington, D.C., U.S. Govt. Printing Office, p. 575–588.

Gallet, S., B.-M. Jahn, B. Van Vliet Lanoe, A. Dia, and E. Rossello (1998), Loess geochemistry and its implications for particle origin and composition of the upper continental crust, *Earth Planet. Sci. Lett.*, *156*, 157–172.

German, C. R., G. P. Klinkhammer, J. M. Edmond, A. Mitra, and H. Elderfield (1990), Hydrothermal scavenging of rare earth elements in the ocean, *Nature*, *345*, 516–518.

German, C. R., N. C. Higgs, J. Thomson, R. Mills, H. Elderfield, J. Blusztajn, A. P. Fleer, and M. P. Bacon (1993), A geochemical study of metalliferous sediment from the TAG hydrothermal mound, 2 608′N, Mid-Atlantic Ridge, *J. Geophys. Res.*, *98*(B6), 9683–9692.

German, C. R., D. L. Bourles, E. T. Brown, J. Hergt, S. Colley, N. C. Higgs, E. M. Ludford, T. A. Nelson, A. Feely, G. Raisbeck, and F. Yiou (1997), Hydrothermal scavenging on the Juan de Fuca Ridge: 230Th, 10Be, and REE's in ridge-flank sediments, *Geochimica et Cosmochimica Acta*, *61*(No. 19), 4067–4078.

German, C. R., J. Hergt, M. R. Palmer, and J. M. Edmond (1999), Geochemistry of a hydrothermal sediment core from the OBS vent-field 21N East Pacific Rise, *Chem. Geol.*, *155*, 65–75.

German, C. R., S. Colley, M. R. Palmer, A. Khripounoff, and G. P. Klinkhammer (2002), Hydrothermal plume-particle fluxes at 13°N on the East Pacific Rise, *Deep Sea Res. I*, *49*, 1921–1940.

Gleason, J. D., T. C. Moore Jr., D. K. Rea, T. M. Johnson, R. M. Owen, J. D. Blum, J. Pares, S. A. Hovan, and C. E. Jones (2002), Ichthyolith Sr isotope stratigraphy of a Neogene red clay sequence: Calibrating eolian dust accumulation rates in the central North Pacific, *Earth Planet. Sci. Lett.*, *202*, 625–636.

Gleason, J. D., T. C. Moore Jr., T. M. Johnson, D. K. Rea, R. M. Owen, J. D. Blum, J. Pares, and S. A. Hovan (2004), Age calibration of piston core EW9709-07 (equatorial central Pacific) using fish teeth Sr isotope stratigraphy, *Palaeogeography, Palaeoclimatology, Palaeoecology*, *212*, 355–366.

Govindaraju, K. (1994), Compilation of working values and description for 383 geostandards, *Geostand. Newsl.*, *18*, 1–158.

Heath, G. R., and J. Dymond (1973), Genesis and transformation of metalliferous sediments from the East Pacific Rise, Bauer Deep, and Central Basin, northwest Nazca Plate, Geological Society of America Bulletin, v. 88, p. 723–733.

Hovan, S. A. (Ed.) (1995), Late Cenozoic Atmospheric circulation intensity and climatic history recorded by eolian depostion in the eastern equatorial Pacific Ocean, Leg 138. Proceedings of the Ocean Drilling Program, Scientific Results.

Ingram, B. L. (1995), High-resolution dating of deep-sea clays using Sr isotopes in fossil fish teeth, *Earth Planet. Sci. Lett.*, *134*, 545–555.

Jones, C. E., A. N. Halliday, D. K. Rea, and R. M. Owen (1994), Neodymium isotopic variations in North Pacific modern silicate sediment and the insignificance of detrital REE contributions to seawater, *Earth Planet. Sci. Lett.*, *127*, 55–66.

Jordahl, K. A., M. K. McNutt, and H. Zorn (1998), Pacific-Farallon relative motion 42–59 Ma determined from magnetic and tectonic data from the Southern Austral Islands, *Geophys. Res. Lett.*, *25*(15), 2869–2872.

Kadko, D. (1985), Late Cenozoic sedimentation and metal deposition in the North Pacific, *Geochimica et Cosmochimica Acta*, *49*, 651–661.

Klinkhammer, G., and A. Hudson (1986), Dispersal patterns for hydrothermal plumes in the South Pacific using manganese as a tracer, *Earth Planet. Sci. Lett.*, *79*, 241–249.

Klinkhammer, G. P., H. Elderfield, J. M. Edmond, and A. Mitra (1994), Geochemical implications of rare earth element patterns in hydrothermal fluids from mid ocean ridges, *Geochimica et Cosmichimica Acta*, *58*(23), 5105–5113.

Kyte, F. T., M. Leinen, G. R. Heath, and L. Zhou (1993), Cenozoic sedimentation history of the central North Pacific: Inferences from the elemental geochemistry of core LL44-GPC3, *Geochmica et Cosmochimica Acta*, *57*, 1719–1740.

Lamarche, G., J.-Y. Collot, R. A. Wood, M. Sosson, R. Sutherland, and J. Delteil (1997), The Oligocene-Miocene Pacific-Australia plate boundary, south of New Zealand: Evolution from oceanic spreading to strike-slip faulting, *Earth Planet. Sci. Lett.*, *148*, 129–139.

Lu, H., Craig S. Fulthorpe, and Michelle A. Mann Paul Kominz (2005), Miocene-Recent tectonic and climatic controls on sediment supply an sequence stratigraphy: Canterbury Basin, New Zealand, *Basin Res.*, *17*, 311–328.

Lyle, M., R. M. Owen, and M. Leinen (1986), History of hydrothermal sedimentation at the East Pacific Rise, 19S, In M. Leinen, D. K. Rea, et al., Initial Reports DSDP, 92: Washington (U. S. Govt. Printing Office), 585–596.

Lyle, M., M. Leinen, R. M. Owen, and D. K. Rea (1987), Late Tertiary history of hydrothermal deposition at the East Pacific Rise, 19S; Correlation to volcano-tectonic events, *Geophys. Res. Lett.*, *14*(6), 595–598.

Maia, M., J. Dyment, and D. Jouannetaud (2005), Constraints on age and construction

process of the Foundation chain submarine volcanoes from magnetic modeling, *Earth Planet. Sci. Lett.*, *235*, 183–199.

Mammerickx, J. (1992), The Foundation Seamounts: Tectonic setting of a newly discovered seamount chain in the South Pacific, *Earth Planet. Sci. Lett.*, *113*, 293–306.

Marchig, V., and J. Erzinger (1986), Chemical composition of Pacific sediments near 20°S: changes with increasing distance from the East Pacific Rise, In M. Leinen, D. K. Rea, et al., Initial Reports DSDP, 92: Washington (U. S. Govt. Printing Office), 371–381.

Marchig, V., J. Erzinger, and H. Rosch (1987), Sediments from a hydrothermal field in the central valley of the Galapagos rift spreading center, *Mar. Geol.*, *76*, 243–251.

McArthur, J. M., R. J. Howarth, and T. R. Bailty (2001), Strontium Isotope Statigraphy: LOWESS Version 3: Best Fit to the marine Sr-Isotope curve for 0-509 Ma and accompanying look-up table for deriving numerical age, *J. Geol.*, *109*, 155–170.

McLennan, S. M. (1989), Rare earth elements in sedimentary rocks: Influence of provenance and sedimentary processes, *Rev. Mineral.*, *21*, 169–200.

Michard, A., F. Albarede, G. Michard, J. F. Minster, and J. L. Charlou (1983), Rare earth elements and uranium in high-temperature solutions from East Pacific Rise hydrothermal vent field (13N), *Nature*, *303*, 795–797.

Mills, R. A., and H. Elderfield (1993), A dual origin for the hydrothermal component in a metalliferous sediment core from the Mid-Atlantic Ridge, *J. Geophys. Res.*, *98*(B6), 9671–9681.

Mills, R. A., and H. Elderfield (1995), Hydrothermal activity and the geochemistry of metalliferous sediment. In: S. E. Humphris, A. Zierenberg, L. S. Mullineaus and R. E. Thomson, Editors, *Seafloor Hydrothermal Systems: Physical, Chemical, Biological and Geological Interactions*, *Geophys. Monogr., Am. Geophys. Union* 91 (1995), pp. 392–405.

Nakai, S. A., A. N. Halliday, and D. K. Rea (1993), Provenance of dust in the Pacific Ocean, *Earth Planet. Sci. Lett.*, *119*, 143–157.

Okal, E. A., and J-M. Bergeal (1983), Mapping the Miocene Farallon Ridge jump on the Pacific plate: A seismic line of weakness, *Earth Planet. Sci. Lett.*, *63*, 113–122.

Owen, R. M., and A. M. Olivarez (1988), Geochemistry of rare earth elements in Pacific hydrothermal sediments, *Mar. Chem.*, *25*, 183–196.

Olivarez, A. M., and R. M. Owen (1989a), REE/FE variations in hydrothermal sediments: Implications for the REE content of seawater, *Geochimica et Cosmichimica Acta*, *53*, 757–762.

Olivarez, A. M., and R. M. Owen (1989b), Plate tectonic reorganizations: Implications regarding the formation of hydrothermal ore deposits, *Mar. Min.*, *6*, 123–138.

Owen, R. M., and D. E. Ruhlin (1986), Interlaboratory comparison of Leg 92 standard sediment sample analyses. In M. Leinen, D. K. Rea, et al., Init. Repts. DSDP, 92: Washington (U. S. Govt. Printing Office), 353–354.

Pettke, T., A. N. Halliday, C. M. Hall, and D. K. Rea (2000), Dust production and deposition in Asia and the north Pacific Ocean over the past 12 Myr, *Earth Planet. Sci. Lett.*, *178*, 397–413.

Pettke, T., A. N. Halliday, and D. K. Rea (2002), Cenozoic evolution of Asian climate and sources of Pacific seawater Pb and Nd derived from eolian dust of sediment core LL44-GPC3, *Paleoceanography*, *17*(3), 1–13, 1031, doi:10.1029/2001PA000673.

Piepgras, D. J., S. B. Jacobsen, and B. Stein (1992), The behavior of rare earth elements in seawater: Precise determination of variations in the North Pacific water column, *Geochimica et Cosmichimica Acta*, *56*, 1851–1862.

Rea, D. K. (1994), The paleoclimate record provided by eolian deposition in the deep sea: The geologic history of wind, *Rev. Geophys.*, *32*, 159–195.

Rea, D. K., and T. R. Janecek (1981), Mass-Accumulation Rates of the non-authigenic inorganic crystalline (eolian) component of the deep-sea sediments from the western mid-Pacific mountains, deep-sea drilling project site 463. Washington, U.S. Government Printing Office.

Rea, D. K., M. Leinen, and T. R. Janecek (1985), Geologic approach to the long-term history of atmospheric circulation, *Science*, *227*, 721–725.

Rea, D. K., et al. (2006), Broad region of no sediment in the southwest Pacific Basin, *Geology*, *34*(10), 873–876.

Revel-Rolland, M., P. De Deckker, B. Delmonte, P. P. Hesse, J. W. Magee, I. Basile-Doelsch, F. Grousset, and D. Bosch (2006), Eastern Australia: A possible source of dust in East Antarctica interglacial Ice, *Earth Planet. Sci. Lett.*, *249*, 1–13.

Rudnicki, M. D., and H. Elderfield (1993), A chemical model of the buoyant and neutrally buoyant plume above the TAG vent field, 26 degrees N, Mid-Atlantic Ridge, *Geochim. et Cosmochim. Acta*, *57*, 2939–2957.

Ruhlin, D. E., and R. M. Owen (1986), The rare earth element geochemistry of hydrothermal sediments from the East Pacific Rise: Examination of a seawater scavenging mechanism, *Geochim. et Comsmochim. Acta*, *50*, 393–400.

Sayles, F. L., T.-L. Ku, and P. C. Bowker (1975), Chemistry of ferromanganoan sediment of the Bauer Deep, *Geol. Soc. Am. Bull.*, *86*, 1423–1431.

Schellart, W. P., G. S. Lister, and V. G. Toy (2006), A late Cretaceous and Cenozoic reconstruction of the Southwest Pacific region: Tectonics controlled by subduction and slab rollback processes, *Earth Sci. Rev.*, *76*, 191–233.

Sherrell, R. M., M. P. Field, and G. Ravizza (1999), Uptake and fractionation of rare earth elements on hydrothermal plume particles at 9deg 45′N East Pacific Rise, *Geochim. et Cosmichim. Acta*, *63*(11/12), 1709–1722.

Smith, J., D. Vance, R. A. Kemp, C. Archer, P. Toms, M. King, and M. Zarate (2003), Isotopic constraints on the source of Argentinian loess - Implications for atmospheric circulation and the provenance of Antarctic dust during recent glacial maxima, *Earth Planet. Sci. Lett.*, *212*, 181–196.

Snoeckx, H., D. K. Rea, C. E. Jones, and B. L. Ingram (1995) Eolian and silica deposition in the central North Pacific: Results from Leg 145 sites 885/885, in: D. K. Rea, I. A. Basov et al. (Eds.), Proceedings of the Ocean Drilling Program, Scientific Results, 145, 219–230.

Stancin, A. M., J. D. Gleason, D. K. Rea, R. M. Owen, T. C. Moore Jr., J. D. Blum, and S. A. Hovan (2006), Radiogenic isotopic mapping of the late Cenozoic eolian and hemipelagic sediment distribution in the east-central Pacific, *Earth Planet. Sci. Lett.*, *248*, 840–850.

Stancin, A. M., J. D. Gleason, D. K. Rea, R. M. Owen, T. C. Moore Jr., J. D. Blum, I. Hendy, and M. Lyle (2007), Fish teeth Sr isotope dating of metalliferous sediment in the SW Pacific Basin, (abstract Fall AGU, San Francisco).

Stein, R., and C. Robert (1985), Siliciclastic sediments at sites 588, 590 and 591: Neogene and Paleogene evolution in the southwest Pacific and Australian climate., *Initial Rep. Deep Sea Drill. Proj.*, *90*, 1437–1454.

Taylor, S. R., and S. M. McLennan (1985), The Continental Crust: its Composition and Evolution, Adlard & Son Ltd.

Taylor, S. R., S. M. McLennan, and M. T. McCulloch (1983), Geochemistry of loess, continental crustal composition and crustal model ages, *Geochim. et Cosmochim. Acta*, *47*, 1897–1905.

Tebbens, S. F., and S. C. Cande (1997), Southeast Pacific tectonic evolution from early Oligocene to present, *J. Geophys. Res.*, *102*(B6), 12,061–12,084.

Walter, H. J., E. Hegner, B. Diekmann, G. Kuhn, and M. M. Rutergs van der Loess (2000), Provenance and transport of terrigenous sediment in the South Atlantic Ocean and their relations to glacial and interglacial cycles: Nd and Sr isotopic evidence, *Geochim. et Cosmochim. Acta*, *64*(22), 3813–3827.

Wells, R. E. (1989), Origin of the oceanic basalt basement of the Solomon Islands arc and its relationship to the Ontong Java Plateau - insights from Cenozoic plate motion models, *Tectonophysics*, *165*, 219–235.

Zhou, L., and T. Kyte Frank (1992), Sedimentation history of the south Pacific pelagic clay province over the last 85 million years inferred from the geochemistry of deep sea drilling project hole 596, *Paleoceanography*, *7*(4), 441–465.

Ziegler, C. L., and R. W. Murray (2007), Geochemical evolution of the central Pacific Ocean over the past 56 Ma, *Paleoceanography*, *22*, PA2203,doi:10.1029/2006PA001321.

Ziegler, C. L., R. W. Murray, S. A. Hovan, and D. K. Rea (2007), Resolving eolian, volcanogenic, and authigenic sediment from the Pacific Ocean, *Earth Planet. Sci. Lett.*, *254*, 416–432.

J. D. Blum, J. D. Gleason, R. M. Owen, D. K. Rea, and A. M. Stancin, Department of Geological Sciences, University of Michigan, Ann Arbor, MI 48109-1005, USA. (jdgleaso@umich.edu)